THE PENNSYLVANIA STATE UNIVERSITY

IONOSPHERIC RESEARCH

Scientific Report No. 349

AN INVESTIGATION OF MASS DISPERSION IN ELECTRIC IMPULSIVE FIELDS

by

H. M. Luther

February 20, 1970

IONOSPHERE RESEARCH LABORATORY

University Park, Pennsylvania NASA Grant NGL 39-009-032

Ionospheric Research

NASA Grant NGL 39-009-032

Scientific Report

on

"An Investigation of Mass Dispersion in Electric Impulsive Fields"

by

H. M. Luther

February 20,, 1970

Scientific Report No. 349

Submitted by: B R F Kendall

B. R. F. Kendall, Project Supervisor

Approved by: G. H. Waynick

A. H. Waynick, Director
Ionosphere Research Laboratory

Ionosphere Research Laboratory

The Pennsylvania State University

TABLE OF CONTENTS

	Page
ABSTRACT	i
I. INTRODUCTION	1
Basic Theory	1
The Impulsive Momentum Integral	2
Effect of the Impulsive Field upon Ion Energy Scatter	6
Mass Dispersion in the Impulsive Field	7
Effect of the Planar Impulsive Field upon Ion Trajectories	9
Summary	10
II. ION ENERGY ANALYSIS	12
The Planar Retarding Grid	12
The Ion Energy Band-Pass Filter	16
The Electrostatic Energy Analyzer	19
III. APPLICATION OF THE PLANAR IMPULSIVE FIELD TO MASS SPECTROMETRY	30
The Constant Momentum Mass Analyzer	30
Resolving Power	32
The Retarding Field CMMA	35
Accelerating Field Constant Momentum Mass Spectrometer	45
Possible Uses for the CMMA	55
APPENDIX - Swept Width Pulse Generator for Impulsive Mass Analyzers	57
BIBLIOGRAPHY	61

ABSTRACT

Ions with energy E_i and a distribution ΔE_i about this energy traversing an impulsive electric field will gain or lose an amount of velocity inversely proportional to their mass. Consequently the final ion energy of the ions in the beam is mass dependent. Further the final ion energy distribution has been broadened or narrowed by a factor which is a function of the impulsive energy gain or loss and the initial ion energy. Ion energy gains and losses in planar and cylindrical impulsive fields are investigated theoretically.

Ion energy analyzers suitable for analyzing energies of ions emerging from impulsive electric fields are discussed theoretically and experimental results are presented. Ion energy analyzers studied include those based on a simple retarding field, the retarding field in combination with an energy bandpass filter, and cylindrical as well as spherical sector fields.

Applications of the mass dispersive properties of the impulsive electric field to mass spectrometry are discussed, and the resolving power as a function of the impulsive field strength and the initial ion energy spread of the ions in a beam incident upon the impulsive field is worked out. Complete impulsive mass spectrometers are described and experimental results are presented. Possible uses of the impulsive mass spectrometer are suggested.

I. INTRODUCTION

1. Basic Theory

Singly charged ions traversing a region to which an electric field of short duration is applied gain or lose an identical impulsive momentum, provided the time duration of the field is less than the time it takes the ions to traverse the region to which the field is applied. Let p_c be this impulsive momentum, then

$$p_c = \int_{\Delta t} e\, \epsilon(t)\, dt \qquad (1)$$

where e is the charge on the ions, $\epsilon(t)$ is the electric field, and Δt is the time duration of the field. After the ions emerge from the impulsive field region, the total ion energy will be

$$E_f = \frac{k}{m} (p_i \pm p_c)^2 \qquad (2)$$

where p_i is the initial ion momentum and the positive sign indicates an impulsive momentum gain while the negative sign indicates a loss. The constant k is 0.483 in a system of units[1] in which time is measured in μ seconds, mass in amu, voltage in volts, energy in eV, and distance in cm. Define the impulsive energy E_c to be

$$E_c = \frac{k}{m} p_c^2, \qquad \text{Def. 1}$$

then with the initial ion energy E_i equation (2) becomes

$$E_f = E_i + E_c \pm 2\sqrt{E_i E_c}\ . \qquad (3)$$

Equation (3) is a generalization of the expression for the energy of an ion emerging from the impulsive electric field derived by J. A. Hipple[10] (1953), V. B. Fiks[11] (1958), J. Bracher[16] (1965), and I. E. Dayton et al[5] (1966) to the case when the initial ion energy is greater than zero.

2. The Impulsive Momentum Integral

Consider now the integral of equation (1). This integral will be evaluated for planar and cylindrical (non-planar) geometries.

The evaluation of the integral in the case of a planar geometry and linear potential is straightforward. Let d be the distance between two grids held at zero potential. After ions have entered the region between the two grids, a voltage $V_c(t)$ is applied to one of the grids for a time τ. The impulsive momentum gained or lost by singly charged ions will then be given by

$$p_c = \pm \frac{e}{d} \int_0^{\tau} V_c(t)dt. \qquad (4)$$

Note that p_c is neither dependent upon the initial ion position at $t = 0$ nor the initial ion energy.

The solution of the integral in cylindrical coordinates can only be obtained approximately. Consider two cylindrical grids having radii R_1 and R_2 with $R_1 < R_2$. Let all distances r be measured from the common axis of the grids to the position of the ions. Assume that singly charged ions are injected radially towards the axis into the region between the grids, and the pulse voltage $V_c(t)$ is applied

to the outer grid for a time τ such that the ions gain an impulsive momentum. Then if p is the ion momentum

$$\frac{dp}{dt} = - \frac{W_c}{r} \tag{5}$$

where $W_c = eV_c/\ln(R_2/R_1)$.

$$\frac{dp}{dt} = \frac{dr}{dt}\frac{dp}{dr} = \frac{p}{m}\frac{dp}{dr}, \tag{6}$$

hence

$$\frac{pdp}{m} = - \frac{W_c dr}{r} \tag{7}$$

from which

$$\frac{p^2}{2m} = - W_c \ln r + K. \tag{8}$$

Let the initial energy of the ions be E_i and let r_i be position of the ions at the instant the pulse is turned on. Note that $R_2 > r_i > R_1$. Then

$$E_i = - W_c \ln r_i + K \tag{9}$$

from which K can be evaluated. Thus

$$E_f = E_i - W_c \ln \frac{r}{r_i} \tag{10}$$

with the restriction that $r_i > r$. The position r as a function of time can be found by solving equation (10) for the momentum p. Then

$$\frac{dr}{dt} = -\sqrt{\frac{2W_c}{m}\left(\frac{E_i}{W_c} - \ln \frac{r}{r_i}\right)}. \tag{11}$$

The minus sign indicates that the ions travel from R_2 towards R_1.

Solving for dt one obtains

$$dt = \frac{-\,dr}{\alpha\sqrt{\Gamma - \ln \frac{r}{r_i}}} \tag{12}$$

where the substitutions

$$\alpha = \sqrt{\frac{2W_c}{m}} \quad \text{and} \quad \Gamma = \frac{E_i}{W_c}$$

have been made. Equation (12) is to be integrated over the pulse duration τ. This, however, cannot be done in closed form. If τ and E_i are not too large, then the final position r_f is not too far away from r_i so that $\ln r/r_i$ can be expanded in a series about r_i

$$\ln \frac{r}{r_i} \sim -\frac{r_i - r}{r_i} + \frac{1}{2}\left(\frac{r_i - r}{r_i}\right)^2 + \ldots . \tag{13}$$

Then

$$\sqrt{\frac{1}{\Gamma - \ln \frac{r}{r_i}}} \sim \sqrt{\frac{1}{\Gamma + \frac{r_i - r}{r_i}}} . \tag{14}$$

Equation (14) may now be expanded to yield

$$\sqrt{\frac{1}{\Gamma + \frac{r_i - r}{r_i}}} \sim \sqrt{\frac{1}{A}}\left[1 + \left(\frac{1}{2A}\frac{r}{r_i} + \ldots\right)\right] \tag{15}$$

where $A = 1 + \Gamma$, hence to first order one obtains

$$dt \sim -\frac{1}{\alpha\sqrt{A}}\left(1 + \frac{1}{2A}\frac{r}{r_i}\right) dr \tag{16}$$

which integrates to

$$\tau \approx \frac{1}{\alpha\sqrt{A}}\left[(r_i - r_f) + \frac{1}{4A}\frac{(r_i - r_f)^2}{r_i^2}\right] . \tag{17}$$

Thus τ to zero order will be

$$\tau \simeq \frac{(r_i - r_f)}{\alpha \sqrt{A}} . \tag{18}$$

Returning now to equation (5), let p_c be the impulsive momentum gain. Then

$$p_c = - W_c \int_o^\tau \frac{dt}{r} . \tag{19}$$

Substituting for dt from equation (16) and integrating yields

$$p_c \simeq \frac{-W_c}{\alpha\sqrt{A}} \left[\frac{r_i - r_f}{2Ar_i} - \ln \frac{r_f}{r_i} \right] . \tag{20}$$

Expansion (13) is used again, and terms are collected to obtain

$$p_c \simeq \frac{-W_c}{\alpha\sqrt{A}} \left(1 + \frac{1}{2A} \right) \left(\frac{r_i - r_f}{r_i} \right) . \tag{21}$$

Solving Equation (18) for $r_i - r_f$ and substituting into equation (21), p_c becomes

$$p_c \simeq - \frac{W_c}{2} \left[\frac{3 + 2(\frac{E_i}{W_c})}{1 + \frac{E_i}{W_c}} \right] \frac{\tau}{r_i} . \tag{22}$$

Note that the impulsive momentum gain in a cylindrical field is dependent both upon the initial ion energy and position. Similarly it can be shown that p_c is a function of r_i and E_i in spherical impulsive fields.

3. Effect of the Impulsive Field Upon Ion Energy Scatter

Returning now to the general problem of ion energy gains and losses in an impulsive field, assume that the ions in the beam incident upon the impulsive field have an energy distribution of width ΔE_i. The final ion energy scatter may be determined from the Taylor-expansion

$$\Delta E_f = \frac{\partial E_f}{\partial E_i} \Delta E_i + \frac{1}{2} \frac{\partial^2 E_f}{\partial E_i^2} \Delta^2 E_i + \ldots \quad . \tag{23}$$

Differentiating equation (3) one obtains, to first order in ΔE_i,

$$\Delta E_f = \Delta E_i \left(1 \pm \sqrt{\frac{E_c}{E_i}}\right). \tag{24}$$

The positive sign indicates an impulsive acceleration, and the negative sign an impulsive deceleration. Thus for an impulsive momentum gain ΔE_f will be greater than ΔE_i, while an impulsive loss decreases the ion energy spread. Note further, that with $E_c = E_i$ $\Delta E_f = 0$ to first order.

The impulsive retarding field has the advantage that it reduces the ion energy spread thus increasing the effective mass dispersion of the impulsive field. Equation (24) is valid for cases where $E_i > \Delta E_i \geq 0$. It can be shown[3], however, that

$$\Delta E_f = \Delta E_i \left(1 \pm 2\sqrt{\frac{E_c}{\Delta E_i}}\right) \tag{24a}$$

when $E_i = 0$.

4. Mass Dispersion in the Impulsive Field

A measure of mass dispersion in an impulsive field will be the change in total ion energy per unit mass increment. Generally the impulsive energy E_c will be given by

$$E_c = \frac{C}{m} \tag{25}$$

where C generally is a function of initial ion energy, the impulsive field strength, the time duration of the field, and the initial position of the ion in the impulsive field. Combining equation (3) with equation (25), one obtains

$$E_f = E_i + \frac{C}{m} \pm 2\sqrt{\frac{E_i C}{m}} \ . \tag{26}$$

A Taylor-expansion of $E_f(m)$ about m yields

$$E_f(m + \Delta m) = E_f(m) - \frac{E_c}{m}\left(1 \pm \sqrt{\frac{E_i}{E_c}}\right)\Delta m + \frac{E_c}{m^2}\left(1 \pm \frac{3}{4}\sqrt{\frac{E_i}{E_c}}\right)\Delta^2 m + \ldots . \tag{27}$$

Thus the change in the total ion energy between mass m and m + 1 will be to the first order in Δm

$$(\Delta E_f)_{\Delta m=1} = -\frac{E_c}{m}\left(1 \pm \sqrt{\frac{E_i}{E_c}}\right) \tag{28}$$

Fig. (1) shows the variation of $(\Delta E_f)_{\Delta m=1}$ as a function of mass m for $m \geq 10$. For such m all terms involving $\Delta^n m$ $(n \geq 2)$ may be neglected. Typical operating parameters are listed on the figure. Note that $(\Delta E_f)_{\Delta m=1}$ in the decelerating field is smaller than in the accelerating field for all masses, other parameters being equal.

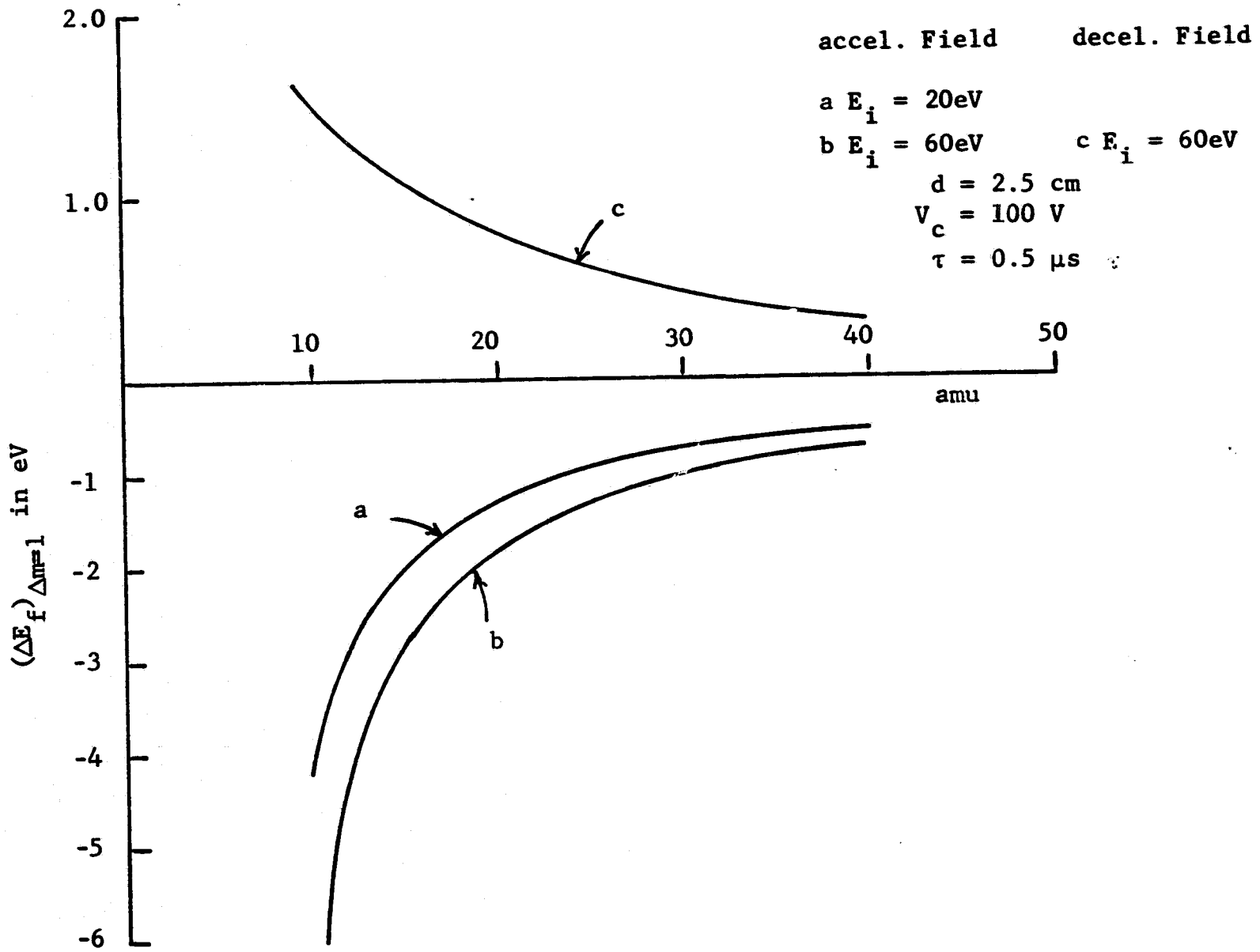

Fig. 1 Mass Dispersion as a Function of Mass

5. Effect of the Planar Impulsive Field Upon Ion Trajectories

Consider an ion in an ion beam traversing a planar impulsive field. Let $\alpha_i(\rho)$ be the tangent of the angle between the initial ion trajectory and the beam axis. α_i will generally be a function of the radial distance ρ from the beam axis. The radial momentum is then

$$p_\rho = p_i \, \alpha_i(\rho) \tag{29}$$

where p_i is the initial ion momentum. Let $\alpha_f(\rho)$ be the tangent of the angle between the final ion trajectory and the beam axis immediately after the ion emerges from the impulsive field,

$$\alpha_f(\rho) = \frac{p_\rho}{p_z \pm p_c} \tag{30}$$

where p_z is the initial ion momentum along the beam axis. If p_z is much larger than p_ρ, then $p_z \sim p_i$. Using this approximation and equation (29) and definition (1), one obtains

$$\alpha_f(\rho) = \left(\frac{1}{1 \pm Q^{1/2}} \right) \alpha_i(\rho) \tag{31}$$

where $Q = E_c/E_i$.

Consider now $\Delta\alpha = \alpha_f - \alpha_i$

$$\Delta\alpha = - \left(\frac{\pm Q^{1/2}}{1 \pm Q^{1/2}} \right) \alpha_i(\rho) . \tag{32}$$

The positive sign must be chosen for an accelerating impulsive field, hence

$$\Delta \alpha_{acc.} < 0;$$

for decelerating fields the negative sign is indicated making

$$\Delta \alpha_{dec.} > 0 .$$

The second inequality shows that the planar impulsive decelerating field defocuses the ion beam. Fig. (2) shows the relative change $\Delta\alpha/\alpha_i$ as a function of Q for the retarding impulsive field.

6. Summary

Four conclusions may be drawn from the preceding analysis:

1. The planar accelerating impulsive field enhances any initial ion energy spread, while the decelerating field decreases the spread.
2. The mass dispersion $(\Delta E_f)_{\Delta m=1}$ is larger for accelerating impulsive fields than for decelerating impulsive fields for constant p_c.
3. Non-collimated ion beams are defocused in the planar decelerating impulsive field.
4. The impulsive momentum gain or loss of an ion traversing a cylindrical impulsive electric field is a function of the initial ion energy and position of the ion within the impulsive field region; while the impulsive momentum gained or lost by ions traversing a planar impulsive field is independent if initial ion energy and position within the field region.

From an experimental viewpoint planar impulsive fields could be used to construct a very sensitive, compact mass-analyzer. The choice between accelerating or decelerating impulsive fields must be determined experimentally on the basis of points 1, 2, and 3.

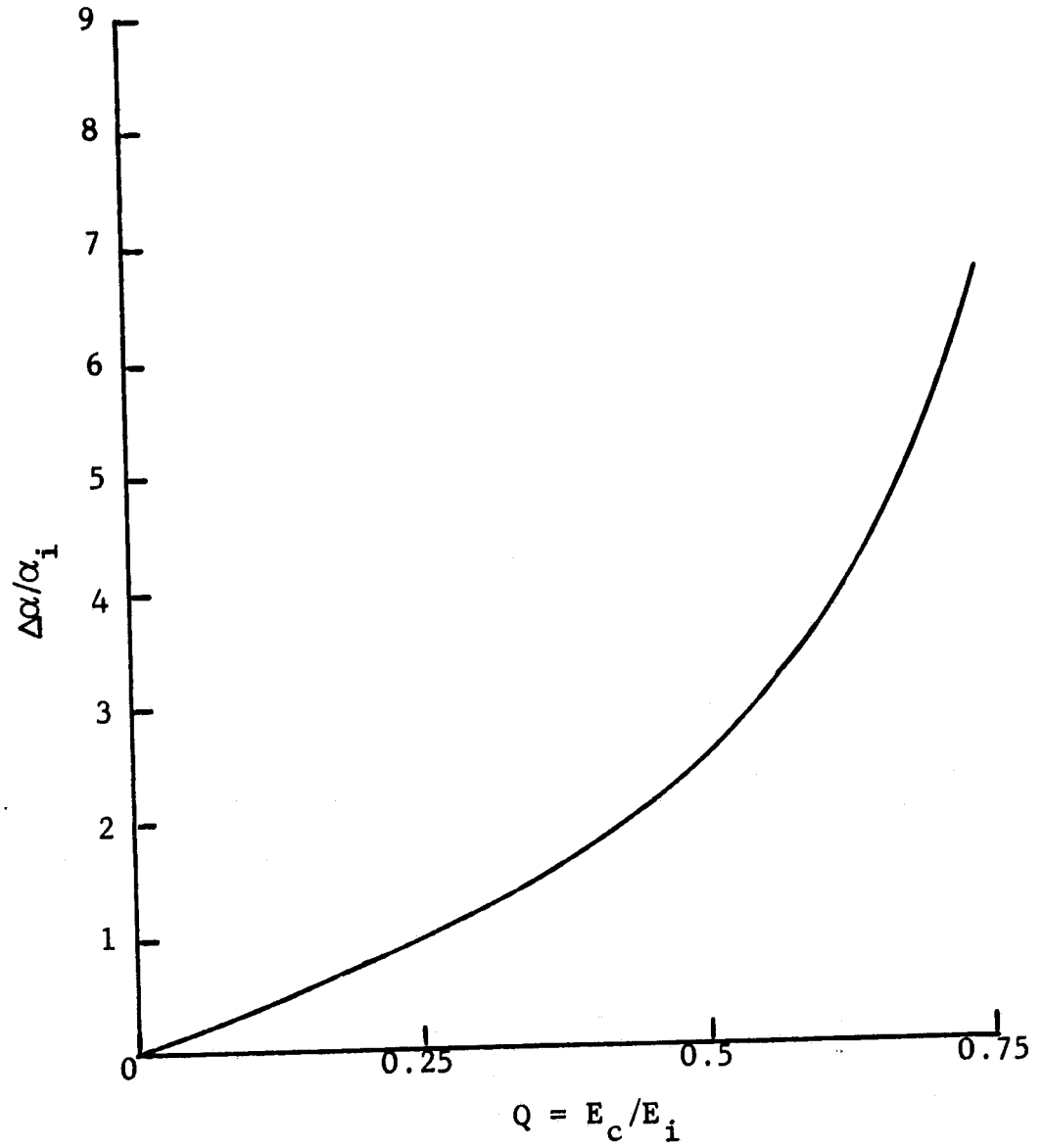

Fig. 2 Change of Ion Trajectory as a Function of Q

II. ION ENERGY ANALYSIS

1. The Planar Retarding Grid

The simplest way to determine ion energies is to apply a retarding voltage $V_r(t)$ in front of the ion current detector, then if $N(E')dE'$ is the number of ions per unit time having energy in the range from E' to $E'+dE'$, the number of ions per unit time arriving at the collector will be given by

$$F_c(V_r) = \int_{E=eV_r}^{\infty} N(E')dE' \qquad (33)$$

from which

$$\frac{dF_c}{dE} = N(E). \qquad (34)$$

The above analysis assumes of course a perfectly collimated ion beam. Generally there will be a small beam divergence which will be enhanced in the retarding field. In order to obtain an estimate of this enhancement, consider an ion having initial energy E_i traversing the region between two grids separated by the distance d. Let z be the direction perpendicular to the grids and ρ the radial distance from the axis of symmetry. A voltage V_r is applied to the grid at $z = d$; the other grid at $z = 0$ is held at zero potential. Thus with the initial conditions $z = 0$ and $\rho = \rho_o$ at $t = 0$ the solution to the equation of motion $m\ddot{\rho} = 0$ and $m\ddot{z} = -eV_r/d$ will be

$$z = v_z t - \frac{eV_r}{2md} t^2 \tag{35a}$$

$$\rho = \rho_o + v_\rho t \ . \tag{35b}$$

Assume $v_z >> v_\rho$, so that $v_z \sim \sqrt{\frac{2E_i}{m}} = v_i$, further with α_i the initial angle of the tangent to the ion trajectory with the system axis, and $E_r = eV_r$ one obtains,

$$z \simeq v_i t - \frac{E_r}{2md} t^2 \tag{36a}$$

$$\rho = \rho_o + v_i \alpha_i t. \tag{36b}$$

When $z = d$, $t = \tau$, then

$$\frac{E_r}{2md} \tau^2 - v_i \tau + d = 0 \tag{37}$$

from which

$$\tau = \frac{v_i \pm \sqrt{\frac{2}{m}(E_i - E_r)}}{\frac{E_r}{md}}$$

$$= \frac{d\sqrt{2m}}{E_r}\left(\sqrt{E_i} \pm \sqrt{E_i - E_r}\right). \tag{38}$$

Since τ must not become unbounded as E_r goes to zero, the minus sign must be chosen. Thus with $\rho_d = \rho_o + v_i \alpha_i \tau$

$$\rho_d = \rho_o + 2d\alpha_i \left(\frac{E_i}{E_r}\right)\left[1 - \sqrt{1 - \frac{E_r}{E_i}}\right] \tag{39}$$

where α_i may in general depend upon ρ_o.

Conservation of charge demands that the current dI_c flowing through a differential area $\rho_o d\rho_o d\phi$ about ρ_o will flow through the area $\rho_d d\rho_d d\phi$, hence

$$J_o(\rho_o)\rho_o d\rho_o d\phi = J_d(\rho_d)\rho_d d\rho_d d\phi \tag{40}$$

from which

$$J_d(\rho_d) = J_o(\rho_o)\,\frac{\rho_o}{\rho_d}\left(\frac{d\rho_d}{d\rho_o}\right)^{-1}. \tag{41}$$

From equation (39) one finds

$$\left(\frac{\rho_o}{\rho_d}\right)\left(\frac{d\rho_d}{d\rho_o}\right)^{-1} = \left[1 + 2\left(\frac{E_i}{E_r}\right)\left(1 - \sqrt{1 - \frac{E_r}{E_i}}\right)x\right.$$
$$\left.\left(\frac{\alpha_i}{\rho_o} + \frac{d\alpha_i}{d\rho_o}\right) + 4d^2\left(\frac{E_i}{E_r}\right)^2\left(1 - \sqrt{1 - \frac{E_r}{E_i}}\right)^2\left(\frac{\alpha_i}{\rho_o}\right)\left(\frac{d\alpha_i}{d\rho_o}\right)\right]^{-1}. \tag{42}$$

Expression (42) is somewhat complex for arbitrary $\alpha_i(\rho_o)$. Consider, however, an ion beam diverging from a point at a distance D from the first grid, then

$$\alpha_i(\rho_o) = \frac{\rho_o}{D}, \tag{43}$$

and equation (42) reduces to

$$\left(\frac{\rho_o}{\rho_d}\right)\left(\frac{d\rho_d}{d\rho_o}\right)^{-1} = \left[1 + \frac{2d}{D}\left(\frac{E_i}{E_r}\right)\left(1 - \sqrt{1 - \frac{E_r}{E_i}}\right)\right]^{-2} \tag{44}$$

so that equation (41) becomes

$$J_d(\rho_d) = J_o(\rho_o)\left[1 + \frac{2d}{D}\left(\frac{E_i}{E_r}\right)\left(1 - \sqrt{1 - \frac{E_r}{E_i}}\right)\right]^{-2}. \tag{45}$$

Note that in the limit as $E_r/E_i \to 0$

$$J_d(\rho_d) \to J_o(\rho_o)\left[1 + \frac{d}{D}\right]^{-2} \tag{46}$$

which agrees with results obtainable from geometric considerations. Fig. (3) shows the experimental verification of equation (45). A surface ionization source[4] provided a diverging beam of ions having an energy E_i. The radial distribution of the ions was measured with an

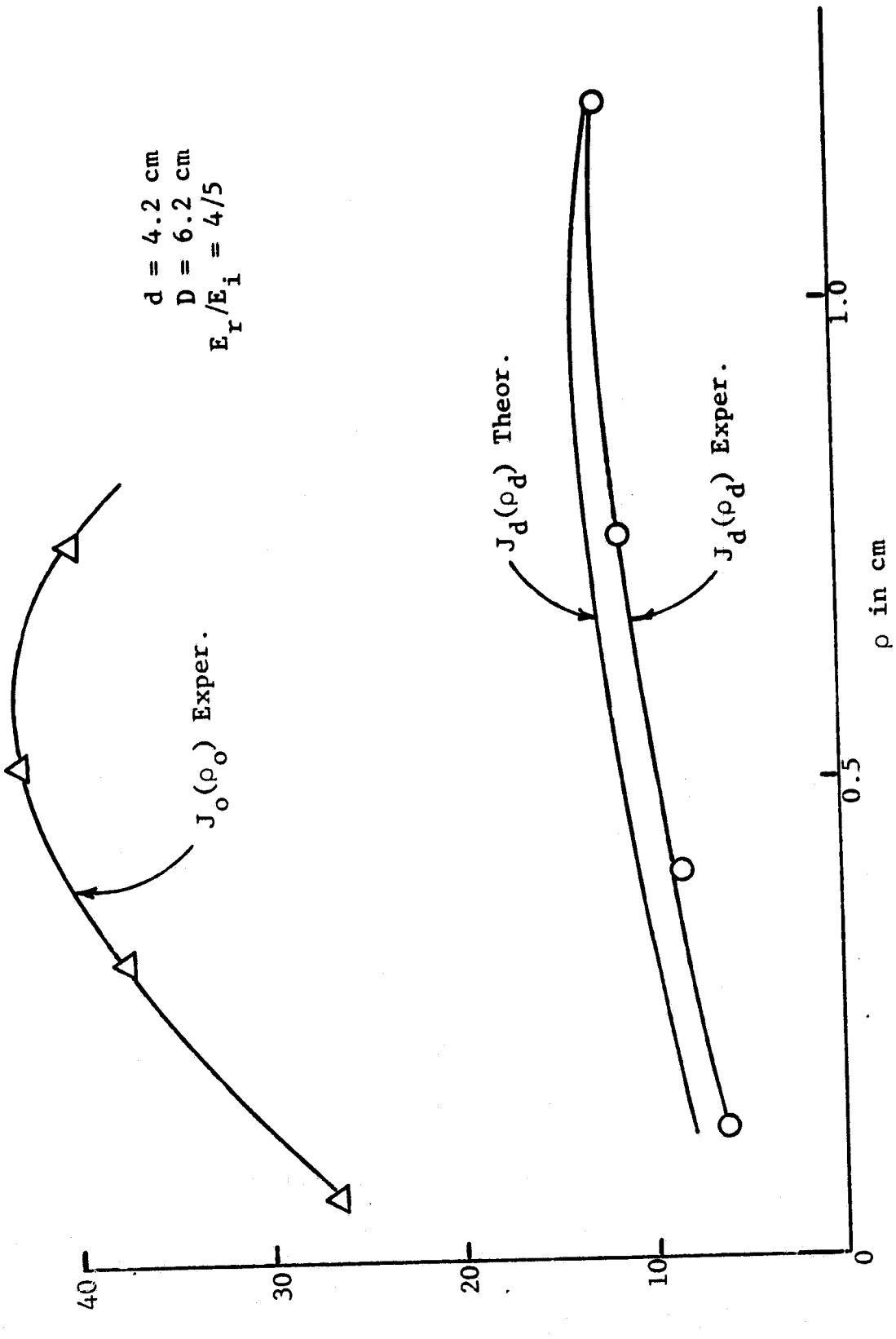

Fig. 3 Defocusing of an Ion Beam by a Planar Retarding Grid

annular ion collector described in a previous paper[4]. Despite the crudeness of the measurements, the agreement is very close over the range of points obtained. Note that the beam impinges slightly off-axis upon the collector. Measurements showed that there was a misalignment of the collimator apertures giving rise to the observed deviation. In order to minimize the undesirable defocusing effect, it is advisable to collimate the ion beam and to make the distance d quite small - of course d has to be kept many times larger than the grid mesh spacing so that the retarding field stays reasonably uniform.

2. The Ion Energy Band-Pass Filter

In the analysis of energy distribution of ions emerging from an impulsive field, it is convenient to set an upper limit E_u to the ion energy of those ions collected so that

$$F_c(V_r) = \int_{E = eV_r}^{E_u} N(E')dE' \quad . \tag{33a}$$

Such an energy band-pass filter was used by I. E. Dayton et al[5] to analyze energies of ions emerging from a 2KV impulsive field, but not discussed in detail.

Consider an ion having energy E_i greater than eV_r incident upon the grids shown in Fig. (4). When the ion enters the region between the slanted electrodes, the equations governing the ion trajectory will be

$$m\ddot{y} = \frac{e}{s}(V_a - V_r) \tag{47a}$$

$$m\ddot{x} = 0 \quad . \tag{47b}$$

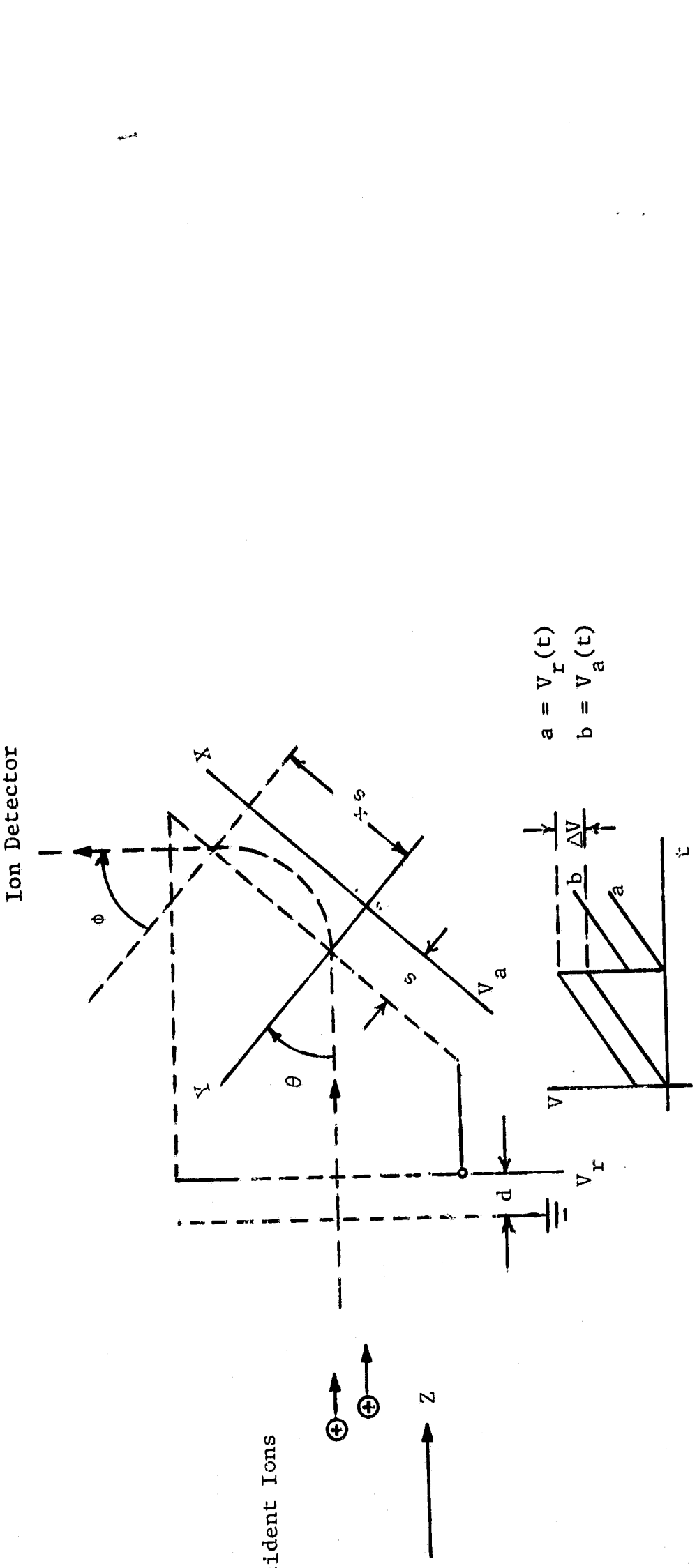

Fig. 4 Ion Energy Band-Pass Filter

A first integration yields

$$m\dot{y} = \frac{e\Delta V}{s}t - m\, v_i\, \beta \tag{48a}$$

$$m\dot{x} = \text{const.} = m\, v_i\, \gamma$$

where $\Delta V = V_a - V_r$, $\beta = \cos\theta$, and $\gamma = \sin\theta$. Integrating equations (48) one obtains

$$y = \frac{e\Delta V}{2ms}\, t^2 - v_i \beta t + s \tag{49a}$$

$$x = v_i \gamma t \ . \tag{49b}$$

Define $E_s = E_i - eV_r$, then an upper limit E_u to E_s is found by demanding that $y = 0$ when $m\dot{y} = 0$. Thus letting $m\dot{y} = 0$ in equation (48a), solving for t and substituting into equation (49a), one obtains

$$y = s\left(-\frac{E_u \beta^2}{e\Delta V} + 1\right) \tag{50}$$

but $y = 0$, hence

$$E_u = \frac{e\Delta V}{\cos^2\theta} \ . \tag{51}$$

Equation (51) expresses the upper limit E_u of E_s in terms of the applied voltages V_r and V_a and the angle of inclination θ .

The angle θ must be chosen such that the collection efficiency of the analyzer-detector does not vary with the ion energy over a range of ion energies. One way to insure this is to adjust θ such that x_s only varies minimally with ion energy. Consider equations (49). Solving equation (49b) for t and substituting into equation (49a) yields

$$y = \frac{e\Delta V\, x^2}{4sE_s\, \gamma^2} - \frac{\beta}{\gamma} x + s \tag{52}$$

When $y = s$, $x = x_s$, hence

$$x_s \left[\left(\frac{R}{4s\gamma^2} \right) x_s - \frac{\beta}{\gamma} \right] = 0 \qquad (53)$$

where $R = e\Delta V/E_s$.

Thus

$$x_s = \frac{4s}{R} \gamma \sqrt{1 - \gamma^2} \ . \qquad (54)$$

Consider small angular deviations from the axis of symmetry; differentiating equation (52) at the point x_s and using equation (53), one obtains

$$\left(\frac{dy}{dx} \right)_{x_s} = \frac{\beta}{\gamma} \ , \qquad (55)$$

hence $\theta = \phi$. This implies that the variations in θ are reflected exactly in ϕ. In order that x_s have an extremal value with respect to γ, one must require that

$$\frac{\partial x_s}{\partial \gamma} = \frac{4s}{R} \frac{(1-2\gamma^2)}{\sqrt{1-\gamma^2}} = 0 \ . \qquad (56)$$

Solving equation (56) for the roots γ_o, one obtains $\gamma_o = \pm 1/\sqrt{2}$. Clearly the choice $\gamma_o = 1/\sqrt{2}$ is indicated, so that the optimum deflection angle θ is 45°. Experimental work using the energy filter is described in section III,3.

3. The Electrostatic Energy Analyzer

The electrostatic sector field has been analyzed in a number of books and articles[6,7,8,9]. This mathematical treatment follows the analyses of Wollnick[7] and Ewald and Liebl[8] as they are the most general

and concise. Consider Fig. (5). R_a, R_b are the radii of curvature of the electrostatic sector field in the vertical direction while r_a, r_b are the radii of curvature in the horizontal direction. Let

$$r_m = \frac{r_a + r_b}{2} \tag{57a}$$

and

$$R_m = \frac{R_a + R_b}{2} \ . \tag{57b}$$

Consider a surface S in the plane of the median trajectory

$$S = R_m \, r_m \, \Delta \phi \, \Delta \theta \tag{58}$$

where $\Delta\theta$ and $\Delta\phi$ are angular displacements in the horizontal and vertical direction respectively. Let S' be a surface differentially displaced in the horizontal direction such that the plane of surface S' is located at a distance $r = r_m(1+\rho)$ and $R = R_m(1+\rho r_m/R_m)$ from the centers of curvature of the electrostatic sector field, then

$$S' = R_m \, r_m \, (1 + \frac{r_m}{R_m} \rho)(1 + \rho) \, \Delta\phi \ \ \Delta\theta \ . \tag{59}$$

Since $\nabla \epsilon = 0$, $\epsilon_o S = \epsilon S'$. Thus

$$\begin{aligned} \epsilon &= \epsilon_o \left[\frac{1}{(1 + \rho)(1 + \frac{r_m}{R_m} \rho)} \right] \\ &= \epsilon_o \left[1 - (1 + \frac{r_m}{R_m} \rho) + \ldots \right] \ . \end{aligned} \tag{60}$$

Hence with $c = r_m/R_m$ the r and z components of ϵ will be

$$\epsilon_r = \epsilon \cos\phi \simeq \epsilon_o \left[1 - (1+C) \, \rho + \ldots . \right] \tag{61a}$$

$$\epsilon_z = \epsilon \sin\phi \simeq \frac{r_m \, \zeta}{R_m(1+c\rho)} \epsilon \tag{61b}$$

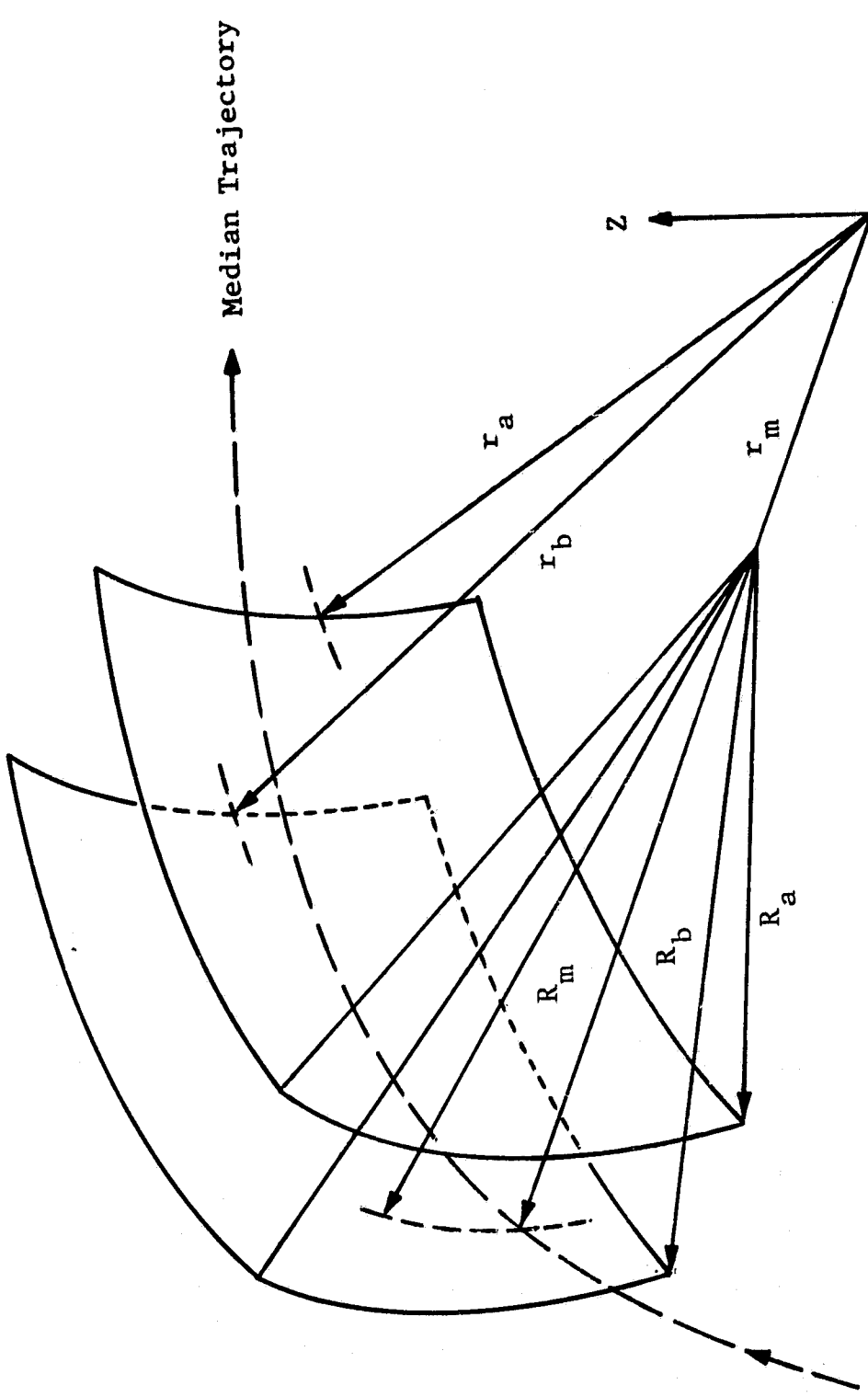

Fig. 5 The Electrostatic Sector Field with Curvature in Two Directions

where $r_m\zeta \sim r_m(1 + \rho)\zeta$ is a small displacement in the vertical direction in the plane of S'. To the first order in ρ and ζ equations (61) reduce to

$$\mathcal{E}_r \sim \mathcal{E}_o \left[1 - (1 + c)\rho\right] \tag{62a}$$

$$\mathcal{E}_z \sim \mathcal{E}_o\, c\, \zeta. \tag{62b}$$

From equations (62) the potential V(r,z) in the neighborhood of the median trajectory is found to be

$$V(r,z) = -\mathcal{E}_o\, r_m \left[\rho - \tfrac{1}{2}(1 + c)\,\rho^2 + \tfrac{1}{2}\, c\, \zeta^2 + \ldots\right] . \tag{63}$$

The equations of motion for a particle having charge e and mass m in the electrostatic sector field are:

$$m\ddot{r} = mr\,\dot{\theta}^2 + e\,\mathcal{E}\,r \tag{64a}$$

$$m\left(\frac{d}{dt}\right)(r^2\dot{\theta}) = 0 \tag{64b}$$

$$m\ddot{z} = e\,\mathcal{E}_z . \tag{64c}$$

A particle on the median trajectory having mass m_o and velocity v_o, will stay on the trajectory provided

$$e\,\mathcal{E}_o = \frac{m_o V_o^{\,2}}{r_m} . \tag{65}$$

Consider next a particle of mass $m = m_o(1 + \gamma)$ entering the sector field with a velocity $v = v_o(1 + \beta)$ on the median trajectory. From the conservation of energy it follows that

$$\frac{m_o(1+\gamma)\, V_o^{\,2}\, (1+\beta)^2}{2} = \frac{m_o(1+\gamma)(1+\beta+\eta)^2\, V_o^{\,2}}{2} + e\, V(r,z) \tag{66}$$

where $\eta = \eta(\rho,\zeta)$. Solving equation (66) for η one obtains

$$\eta^2 + 2(1+\beta)\eta + 2A(1-\gamma) = 0 \tag{67}$$

where $A = \rho - 1/2(1+c)\rho + 1/2\ c\rho^2$. η, however, is a differential quantity which goes to zero with ρ and ζ, so that neglecting the η^2 term one obtains

$$\eta(\rho,\zeta) = -A(1-\beta-\gamma). \tag{68}$$

Hence the particle velocity in the neighborhood of the median trajectory will be to second order

$$v = v_o\left[1+\beta-\rho + \tfrac{1}{2}c(\rho^2-\zeta^2) + \tfrac{1}{2}\rho^2 + \rho(\gamma+\beta)\right] \tag{69}$$

From equation (69) one obtains θ to first order

$$\dot{\theta} = \frac{V}{r} \simeq \frac{v_o}{r_m}(1+\beta-2\rho). \tag{70}$$

Inserting expression (62a), (65), and (70) into equation (64a) yields

$$\begin{aligned} m_o(1+\gamma)r_m\rho = m_o(1+\gamma)r_m\ (1+\rho)\ x \\ \left(\frac{V_o}{r_m}\right)^2 (1+2\beta-4\rho) - r_m m_o\left(\frac{V_o}{r_m}\right)^2\left[1-(1+c)\rho\right] \end{aligned} \tag{71}$$

which can be reduced to

$$\ddot{\rho} = \left(\frac{V_o}{r_m}\right)^2 \kappa^2(\delta-\rho) \tag{72}$$

where $\kappa = \sqrt{2 - c}$, and $\delta = (2\beta+\gamma)/\kappa^2$. The first order equation of motion in the vertical plane may be derived by inserting equation (65) into (64c) and simplifying the resulting equation to obtain

$$\ddot{\zeta} = -\left(\frac{V_o}{r_m}\right)^2 c\ \zeta\ . \tag{73}$$

Equations (72) and (73) may be solved using standard techniques. The solutions, of course, are oscillatory and have the form:

$$\rho(t) = \rho_o \sin(\kappa\omega t + \alpha_1) + \delta \tag{74a}$$

$$\zeta(t) = \zeta_o \sin(\sqrt{c}\,\omega t + \alpha_2) \tag{74b}$$

where $\omega = V_o/r_m$, α_1, α_2 are phase angles and ρ_o, ζ_o are amplitudes dependent upon initial conditions. Consider $\dot{\rho}(t) = \kappa\,\omega\,\rho_o \cos(\kappa\,\omega t + \alpha_1)$. For some $t = t_1, \dot{\rho}(t) = \dot{\rho}(t + t_1)$, hence $\omega t_1 = \pi/\kappa$. Thus the horizontal deflection angle $\Theta = \pi/\kappa c$; similarly the vertical deflection angle $\Phi = \pi/\sqrt{c}$. There are two special cases of interest: R_m is infinite, and $R_m = r_m$. The former is the cylindrical sector field for which $c = 0$ so that $\Theta = \pi/\sqrt{2} = 127°\ 17'$. Note that there is no focusing action in the vertical plane. The latter case is the spherical sector for which $\Theta = \Phi = \pi$. This sector field focuses the charged particles in both planes. The focusing properties of the sector field will in practice be affected by the fringing fields at the entrance and exit of the sector. The effect of the fringing field can be minimized by suitably shielding the entrance and exit of the sector with a grounded plate. The mathematical analysis of the shielding diaphragms and their position relative to the sector is given by H. Wollnick[7].

Equation (66) shows that only ions having an energy in the neighborhood of $E_o = e\,\epsilon_o r_m/2$ may be transmitted. Thus the electrostatic sector field is a convenient energy analyzer. A cylindrical and a spherical electrostatic energy analyzer (EEA) have been

constructed. Figs. (6) and (8a) show the cylindrical EEA and a typical energy spectrum obtained with an electron beam incident upon the analyzer respectively. Figs. (7) and (8b) show a spherical EEA and energy spectrum obtained by using the same electron source. The thermal spread of the electrons is approximately 0.2eV at typical operating temperatures of the filament. Considering the above to be the true energy spread of the electrons, Fig. (9) shows that the resolutions of the cylindrical and the spherical EEA are approximately 0.5eV and 0.9eV respectively.

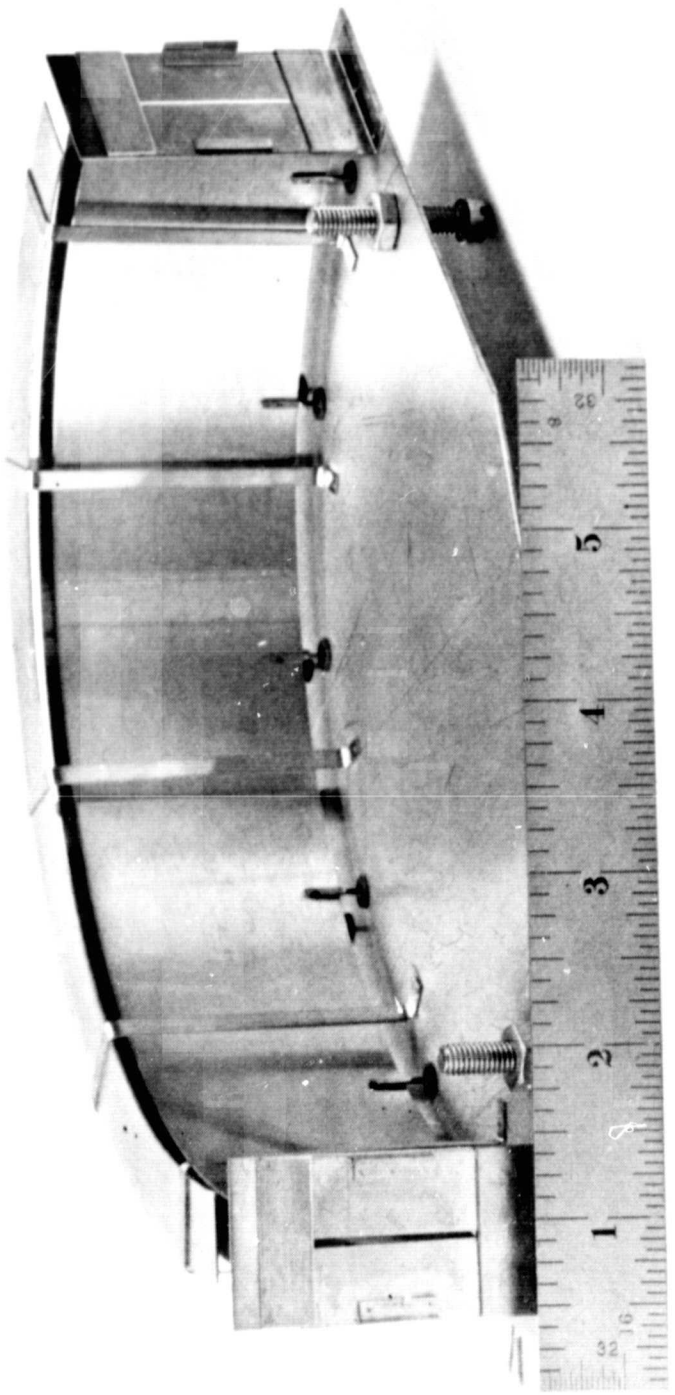

Fig. 6 Cylindrical Electrostatic Sector Field

Fig. 7 Spherical Electrostatic Sector Field with Interchangeable Slits and Ion Collector

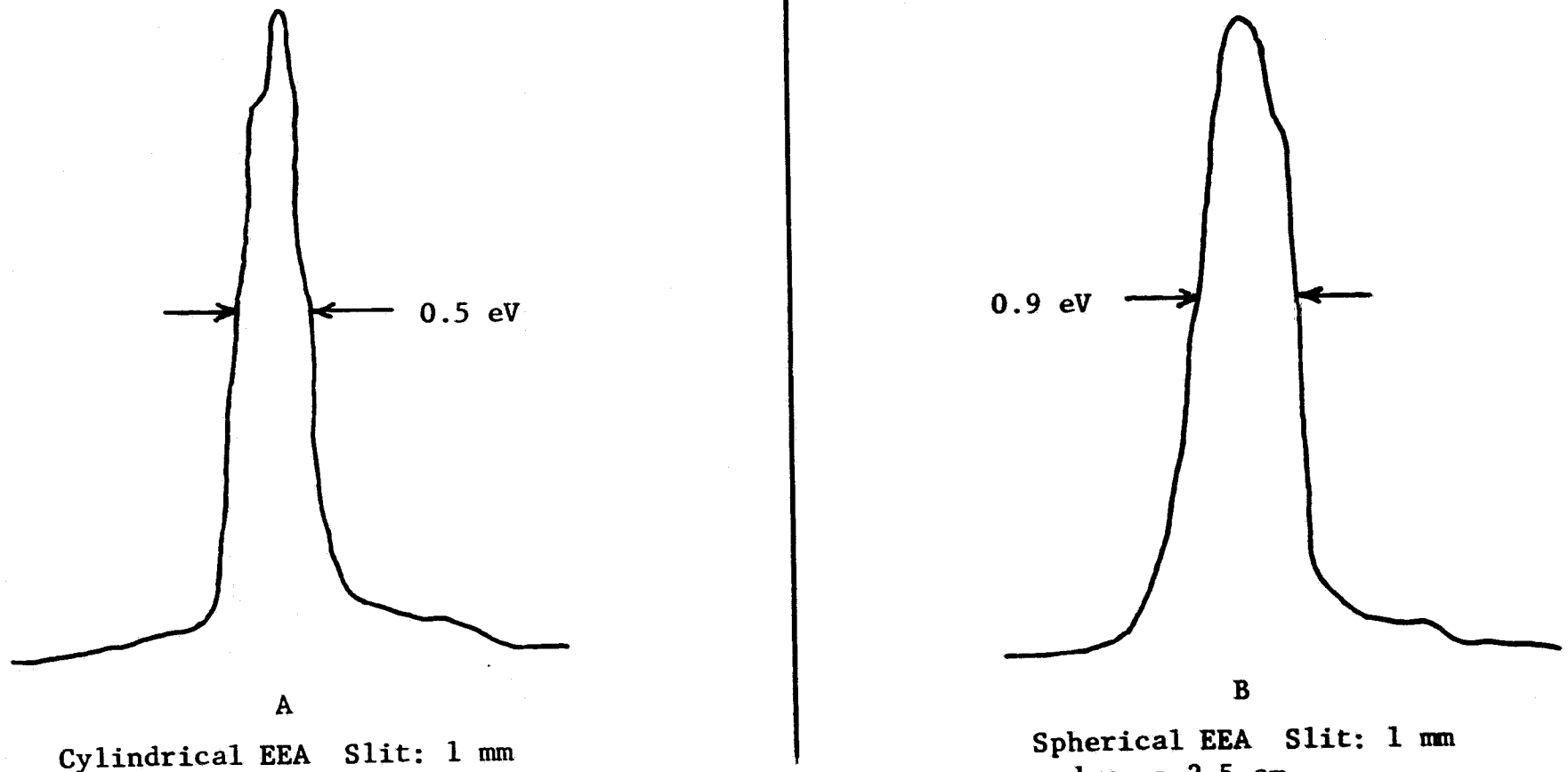

A

Cylindrical EEA Slit: 1 mm
and r_m = 10.5 cm

B

Spherical EEA Slit: 1 mm
and r_m = 2.5 cm

Fig. 8 Typical Energy Spectra Obtained with EEA

EEA	r_a	r_b	Θ	V_+^*	V_-^*	slit width
cylind.	10 cm	11 cm	127.2°	0.2 V_{acc}	0.2 V_{acc}	1 - 3 mm
spher.	2 cm	3 cm	180°	0.3 V_{acc}	0.5 V_{acc}	1 - 2 mm

* in terms of the accelerating voltage V_{acc} of the ions or electrons incident upon EEA.

Fig. 9 Operating Parameters of the Cylindrical and Spherical EEA

III. APPLICATION OF THE PLANAR IMPULSIVE FIELD TO MASS SPECTROMETRY

1. The Constant Momentum Mass Analyzer

The mass dispersive characteristics of the planar impulsive field may be used to good advantage in performing mass analysis. Figure (10), which is taken from Hipple's patent[10], shows how a planar impulsive field and an ion energy analyzer may be combined to function as a constant momentum mass analyzer (CMMA). The CMMA was originally proposed by J. A. Hipple[10] in 1953. A later paper by V. B. Fiks[11] proposed the same device. In 1958 W. M. Brubaker[12] patented a CMMA consisting of two cylindrical EEA's and a planar accelerating impulsive field. One EEA was placed in front of the impulsive field in order to reduce the initial energy spread ΔE_i of ions entering the impulsive field. The other EEA was positioned behind the impulsive field to analyze the energies of ions emerging from the impulsive field. None of the above, however, reported any experimental work on the analyzer.

Experimental work on constant momentum mass analyzers had its beginnings in 1953 when M. M. Wolff and W. E. Stephens[13] used an impulsive accelerating field to construct a time of flight mass analyzer with a linear mass scale. In 1959 B. R. F. Kendall[14,15] worked on a CMMA consisting of a planar accelerating impulsive field and a cylindrical EEA. He, however, did not obtain an adequate resolving power from the instrument. In 1965 a constant momentum mass analyzer composed of a planar impulsive accelerating field and

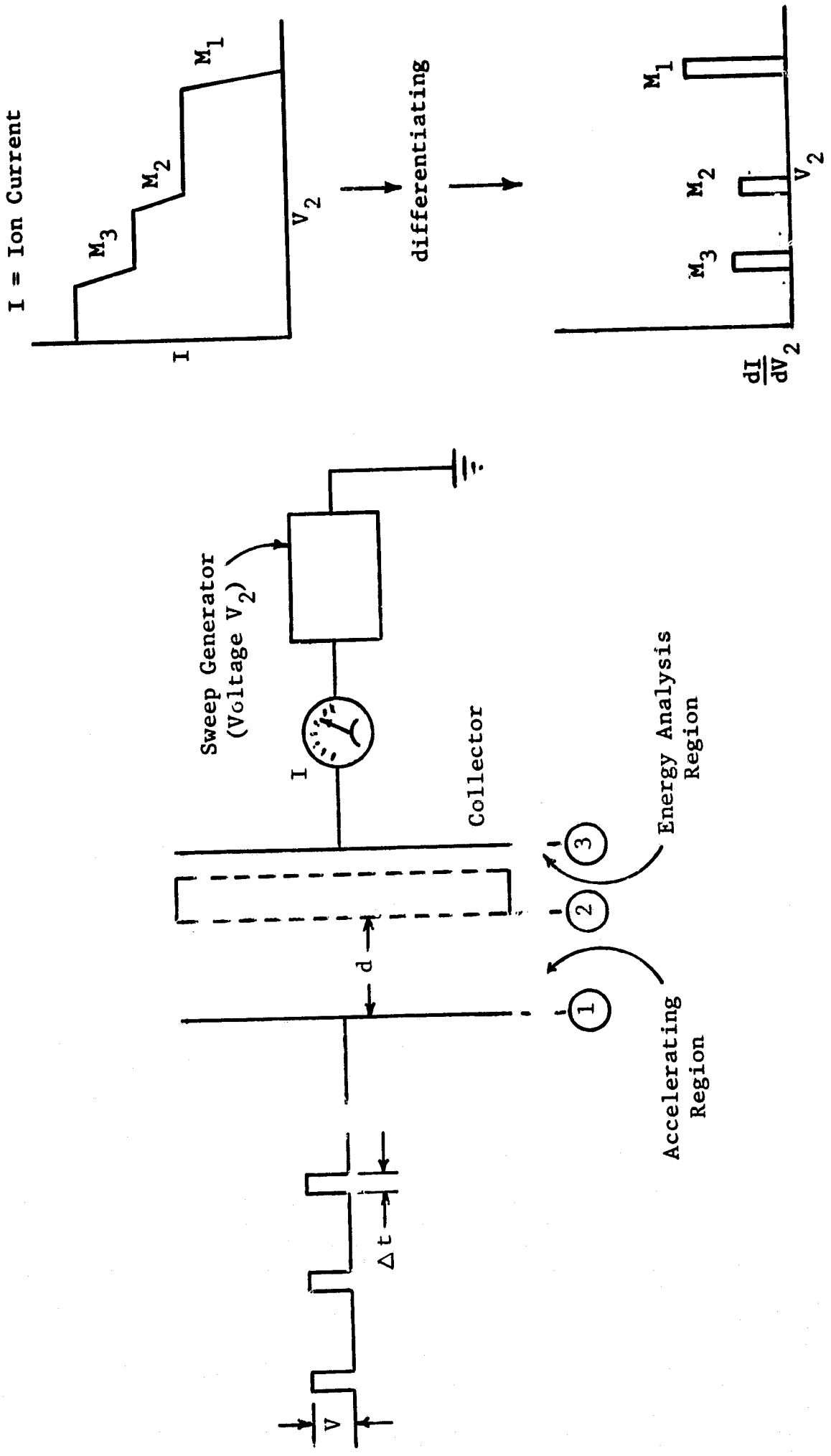

Fig. 10 Basic Constant Momentum Mass Analyzer

cylindrical electrostatic energy analyzer was described by J. Bracher[16]. A year later I. E. Dayton[5] published a report on an operational CMMA having a somewhat lower resolving power but a higher sensitivity than Bracher's instrument. The same year H. M. Luther reported on a CMMA having a resolving power comparable to that obtained by the other workers; this analyzer, however, does not require the extreme pulse voltages of both Bracher's and Dayton's instruments. Further experiments by Luther have led to an analyzer which is described in section III.4. The mass analyzers are all compared in the chart on Fig. (11). All spectrometers listed in the chart are of the accelerating type.

2. Resolving Power

There are currently two definitions for the resolving power of a mass analyzer in use. The resolving power at mass m is defined to be

$$R(m) = \left|\frac{m}{\Delta m}\right| \qquad \text{Def. 2}$$

where Δm is the width of the mass peak in mass units. The resolving power may also be defined as that mass at which an adjacent peak can just be resolved. This definition is a special case of definition 2 and is obtained by requiring Δm to be equal to 1 amu. Then the resolving power R_o is equal to the numerical value of the mass m_o

$$R_o = |m_o| \qquad \text{Def. 3}$$

Consider equation (28). Solving for the numerical value of $m/\Delta m$ one obtains

Mass Analyzer	Energy Analyzer*	Pulse Voltage	Total Ion Flight path	Resolving Power	Mass Sensitivity
Bracher	A(Z)	3 KV	25 cm	30	0.1 A/Torr
Dayton	C	2 KV	10 cm	> 15	3 A/Torr
Luther I	B	100 V	8 cm	20	-
Luther II	A(S)	100 V	14 cm	12	10^{-15} A ion^{-1} cm^{3} †

* A - EEA; (Z) cylindrical, (S) spherical
B - Simple Retarding Grid
C - B plus Energy Band-Pass Filter

† Depends upon Pulse Repetition Frequency

Fig. 11 Comparison of Constant Momentum Mass Analyzers

$$\left|\frac{m}{\Delta m}\right| = \frac{E_c}{\Delta E_f(m)} \left|1 \pm \sqrt{\frac{E_i}{E_c}}\right|. \qquad (75)$$

If the ion energy analyzer has an energy resolution of ϵ and assuming that ϵ is independent of the ion energy, then the resolving power R(m) of the mass spectrometer will be

$$R(m) = \frac{E_c}{\epsilon} \left|1 \pm \sqrt{\frac{E_i}{E_c}}\right| \qquad (76)$$

in the absence of any initial energy scatter of the incident ions. Assume now that the incident ions have an energy spread ΔE_i. This spread is broadened according to the equation (24). Thus the effective resolving power $R(m,\Delta E_i)$ will be given to first order in $\frac{\Delta m}{m}$ by

$$R(m,\Delta E_i) = \frac{E_c \left|1 \pm \sqrt{\frac{E_i}{E_c}}\right|}{\epsilon + \Delta E_i \left|1 \pm \sqrt{\frac{E_c}{E_i}}\right|}. \qquad (77)$$

where, as before, the positive sign is indicated for an accelerating impulsive field and the minus sign is indicated for the decelerating impulsive field.

Consider the accelerating case of equation (77). Let E_c get very large. Then

$$R_m(\Delta E_i) \rightarrow \frac{E_c}{\sqrt{\frac{E_c}{E_i}}\,\Delta E_i}, \qquad (78)$$

so that for very large E_c it can be shown[3] that

$$R_o(\Delta E_i) \sim V_c^{2/3} \tag{79}$$

where V_c is the impulsive field voltage of the planar impulsive field. This dependence is in general agreement with Bracher's[16], presumably empirical, determination of

$$R_o(\Delta E_i) \sim V_c^{1/2}. \tag{80}$$

It is experimentally convenient to define the measurable resolving power $R_{exp}(m)$ of the spectrometer as

$$R_{exp}(m) = \left[\frac{E_c \left| 1 \pm \sqrt{\frac{E_i}{E_c}} \right|}{\Delta E(m)} \right] 0.5 \tag{81}$$

where the subscript 0.5 indicates that the measurement of $\Delta E(m)$ is made at the half-height of the mass peak. Note that as E_i approaches zero

$$R_{exp}(m) \rightarrow \left[\frac{E_c}{\Delta E(m)} \right] 0.5 \tag{81a}$$

which is the experimental resolving power as defined in a previous publication[3].

3. The Retarding Field CMMA

In section I,6 it was observed that the width of the ion energy distribution of ions emerging from a decelerating impulsive field was smaller than the width of the initial ion energy spread. This observation led to a series of experiments designed to evaluate the performance of a decelerating field CMMA. Tests evaluating the performance of a gated decelerating field CMMA have been described

previously[3]. It was seen that both mass sensitivity and resolving power were low. In order to determine the reason for this deficiency, an ungated mass spectrometer was constructed using parts from an electron - optical kit[4]. Fig. (12) shows the essential details of the spectrometer. A surface ionization source[4] charged with Na and K salts provided an ion beam of about 10^{-9} A incident upon the mass analyzer. The impulsive field region measured 2.5 cm, and the total ion flight path was 8 cm. The pulse divider network shown in the upper left hand corner of Fig. (12) insured a spatially linear decelerating field, while the capacitors $C_{1..4}$ were used to correct any distortions in the pulse shape due to stray capacitance in the resistor chain. The dashed curve in Fig. (13) shows the energy distribution about E_i = 12eV of the ions incident upon the analyzer. Before the retarding pulse voltage $V_c(t)$ was turned on, the voltage applied between the electrodes of the energy band pass filter was adjusted such that no ions having energy greater than E_i were collected. The magnitude of ΔV = 6V determined experimentally was found to agree with equation (51) within a few percent.

The performance of the spectrometer verified qualitatively the predictions made in sections I,4 and I,5. For $E_c \sim E_i$ the collector current was attenuated by a factor of 10^3, and the mass dispersion was barely large enough to separate the Na^+ and K^+, the two components of the incident ion beam. The solid line in Fig. (13) shows the mass spectrum. The experimental resolving power at mass 40 was found to be about 3 which is in agreement with the theoretical prediction based on equation (77). The reason for the low resolving power of the retarding

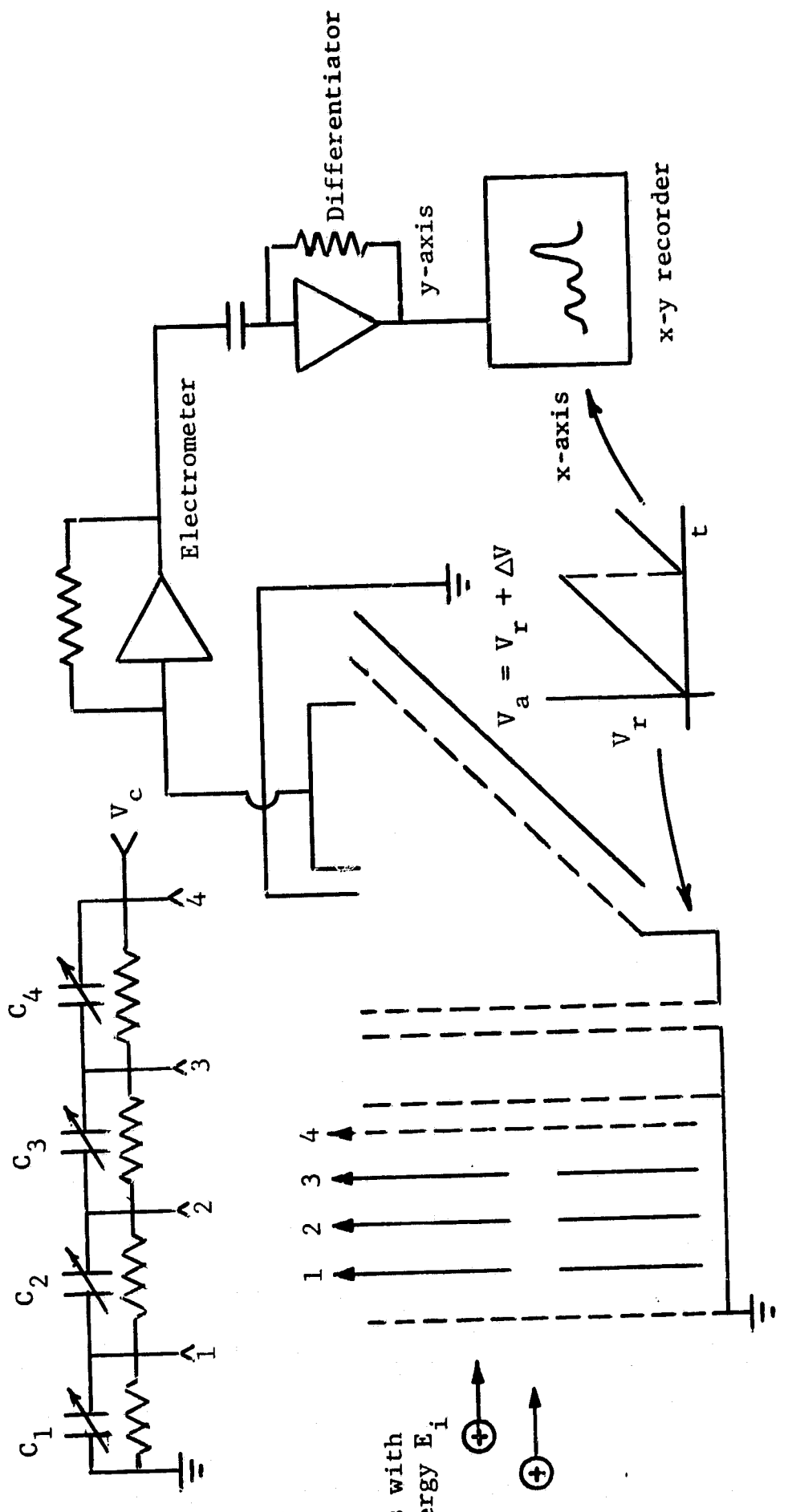

Fig. 12 Decelerating Field Constant Momentum Mass Analyzer

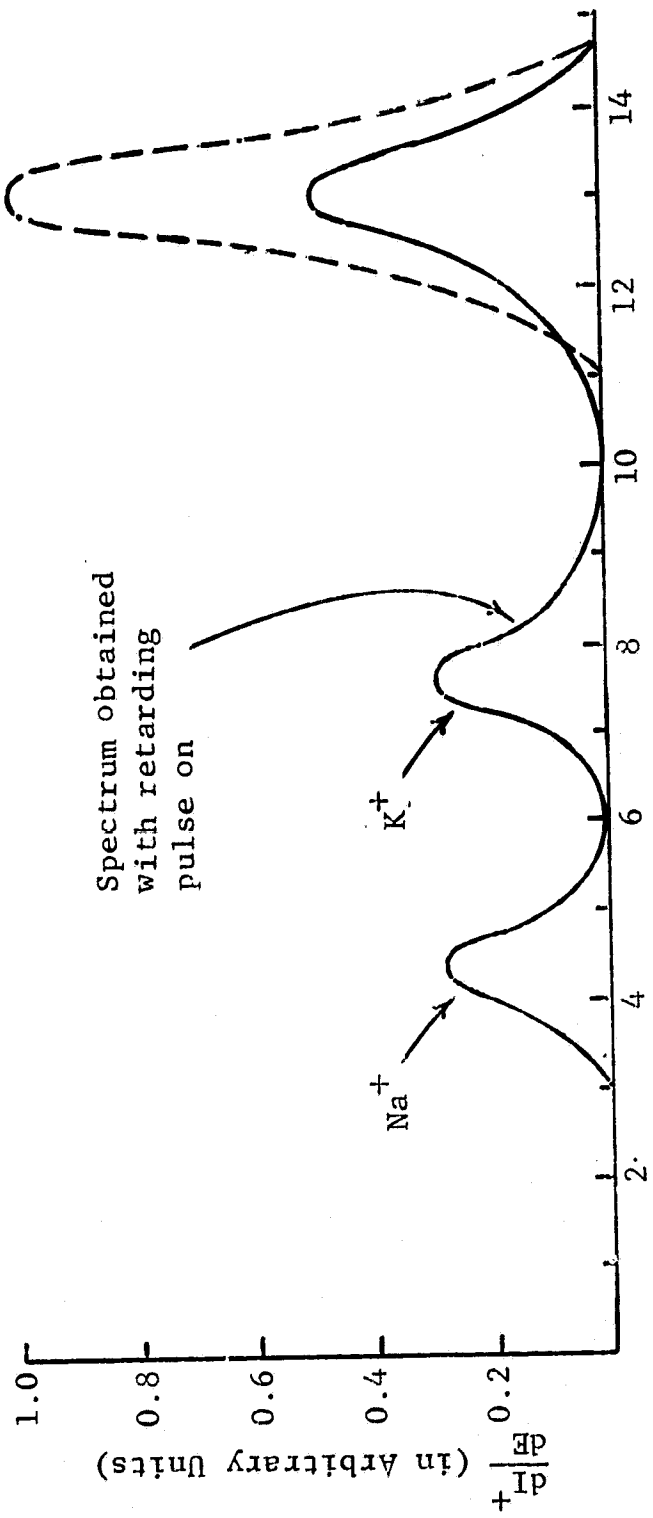

Fig. 13 Typical Mass Spectrum

field CMMA is thus seen to be a consequence of the fact that to first order in Δm.

$$\text{Lim } R(m,\Delta E_i) = 0 \quad \text{as } E_i/E_c \to 1 \tag{82}$$

provided ϵ is independent of the final ion energy, while its low sensitivity is seen to be caused by the defocusing effect of the decelerating impulsive field.

There is, however, another mode of operation of the retarding field CMMA which relies on the defocusing effect mentioned in section I,4. The geometry of this spectrometer is shown in Fig. (14). Consider an ion beam incident upon the impulsive field region at an angle α_i with respect to the normal of the field region. Analogous to the development in section I,5

$$\tan \alpha_f = \frac{p_\rho}{p_z - p_c} , \tag{83}$$

hence

$$\tan \alpha_f = \frac{\sin \alpha_i}{\cos \alpha_i - Q^{1/2}} \tag{84}$$

where, as before, $Q = E_c/E_i$.

Consider now the ray reaching the collector. The angle α_f of this particular ray is $\pi/2$ so that $\tan \alpha_f = \infty$ from which it follows that

$$E_c = E_i \cos^2 \alpha_i . \tag{85}$$

Consider now the integral in equation (4). If $V_c(t)$ is a square pulse, then with $b = k(eV_c/d)^2$ one obtains

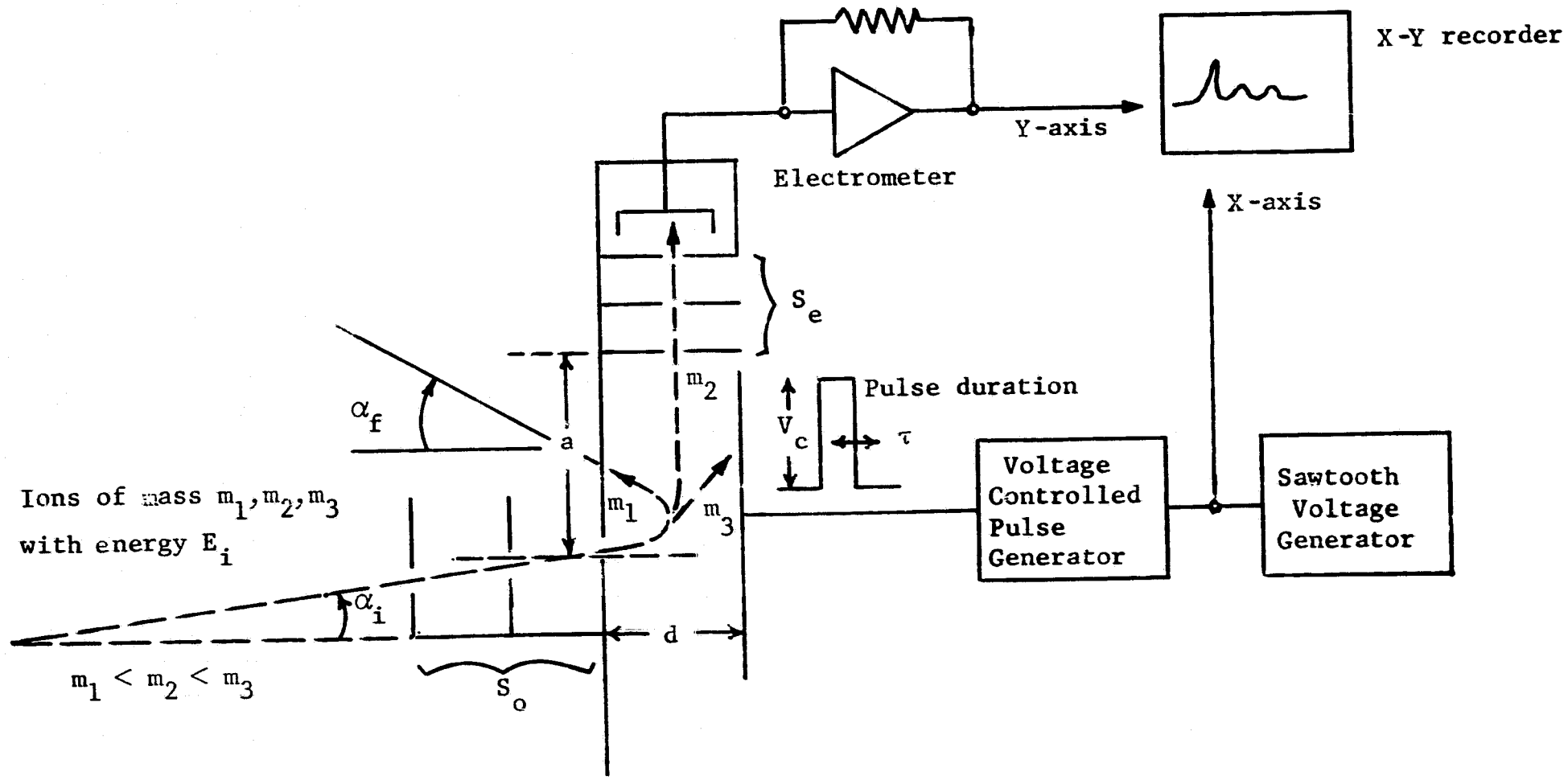

Fig. 14 Proposed Decelerating Constant Momentum Mass Analyzer

$$E_c = \frac{b\tau^2}{m} \tag{86}$$

where τ is the time duration of the decelerating pulse. Combining equations (85) and (86) one obtains after rearranging terms

$$m = \frac{b\tau^2}{E_i} (1 + \tan^2 \alpha_i) \tag{87}$$

Consider now a Taylor-expansion of $m(\tau,E_i,\alpha_i)$ about (t,E_i,α_i)

$$\begin{aligned} m(\tau+\Delta\tau,E_i+\Delta E_i,\alpha_i+\Delta\alpha_i) &= m(\tau,E_i,\alpha_i) + \\ m\left[\frac{2\Delta\tau}{\tau} - \frac{\Delta E_i}{E_i} + 2\tan\alpha_i\ \Delta\alpha_i\right] &+ \ldots, \end{aligned} \tag{88}$$

hence to first order in $\Delta\tau$, ΔE_i, and $\Delta\alpha_i$

$$\Delta m = m\left[\frac{2\Delta\tau}{\tau} - \frac{\Delta E_i}{E_i} + 2\tan\alpha_i\ \Delta\alpha_i\right] . \tag{89}$$

If a perfectly collimated, mono-energetic ion beam were incident upon the mass analyzer, the maximum obtainable resolving power R(m) would be

$$R(m) = \frac{1}{2}\left(\frac{\tau}{\Delta\tau}\right) . \tag{90}$$

In the presence of angular deviation $\Delta\alpha_i$ about α_i and an energy spread ΔE_i about E_i, the resolving power $R(m,\Delta E_i,\Delta\alpha_i)$, however, becomes

$$R(m,\Delta E_i,\Delta\alpha_i) = \frac{R(m)}{1 + R(m)(\epsilon_1 + 2\epsilon_2)} \tag{91}$$

where $\epsilon_1 = \left|\Delta E_i/E_i\right|$ and $\epsilon_2 = \left|2\tan\alpha_i\ \Delta\alpha_i\right|$. Note that the factor 2 multiplying ϵ_2 takes into account a symmetric angular distribution of the ion trajectories about α_i, while ΔE_i is not doubled, since it was chosen symmetrically about the energy E_i. It is clear from the form of ϵ_1 that the initial energy should be made large in order to make

ϵ_1 small. The angle α_i, however, may not be chosen arbitrarily, since it depends upon the required pulse generator duty cycle, defined as the ratio of the pulse duration τ to the period T of the output voltage $V_c(t)$, the initial ion energy E_i and the physical dimensions of the analyzer. In order to derive an explicit expression for α_i in terms of the above parameters, consider an ion with a mass M which is at the upper limit of the dynamic mass range of the mass analyzer. This ion must traverse the distance a shown in Fig. (14) within a time interval smaller than T. T is related to duty cycle δ and the pulse duration τ by the equation

$$T = \frac{\tau}{\delta} . \tag{92}$$

Let δ_M be the duty cycle corresponding to the mass M, then the time interval t of transit of the ion having mass M must be related to δ_M in the following way

$$t = \frac{M\,a}{\sqrt{2\,M\,E_i\,\sin\alpha_i}} \leq \frac{\tau_M}{\delta_M} = T. \tag{93}$$

Consider now the central inequality of equation (93). Assume the limiting case, then equating the two terms and substituting equations (85) and (86) into equation (93) one obtains after simplifying

$$\sin^4\alpha_i - \sin^2\alpha_i + \frac{b}{2}\left(\frac{a\delta_M}{E_i}\right)^2 = 0. \tag{94}$$

Recall that

$$b = k\left(\frac{eV_c}{d}\right)^2 \tag{95}$$

for a square pulse $V_c(t)$. Using equation (95) in equation (94) and

solving for sin α_i, one obtains

$$\sin \alpha_i = \frac{1}{\sqrt{2}} \left[1 \pm \sqrt{1 - 2k \left(\frac{aV_c}{dV_i} \right)^2 \delta_M^2} \right]^{1/2} . \qquad (96)$$

The negative root has been discarded, since only positive angles are of interest. The discriminant appearing in equation (96) yields the maximum duty cycle Δ_M at mass M in terms of the geometrical parameters a and d, the impulsive voltage V_c, and the accelerating voltage V_i.

$$\Delta_M = \frac{1}{\sqrt{2k}} \left(\frac{dV_i}{aV_c} \right) . \qquad (97)$$

Thus equation (96) may be simplified using equation (97) to yield

$$\sin\alpha_i = \frac{\sqrt{2}}{2} \left[1 \pm \sqrt{1 - \left(\frac{\delta_M}{\Delta_M} \right)^2} \right]^{1/2} . \qquad (98)$$

Consider now the case when $\delta_M << \Delta_M$. Expanding equation (98) to first order and collecting terms yields two solutions $\sin \alpha_i^+$ and $\sin \alpha_i^-$

$$\sin \alpha_i^+ \simeq \left[1 - \left(\frac{\delta_M}{2\Delta_M} \right)^{2} \right]^{1/2} \qquad (99a)$$

$$\sin \alpha_i^- \simeq \frac{1}{2} \left(\frac{\delta_M}{\Delta_M} \right) . \qquad (99b)$$

Let $\alpha_i^+ = \pi/2 - \gamma$, then it follows from an expansion of $\sin \alpha_i^+$ that

$$\gamma \simeq \frac{1}{2} \frac{\delta_M}{\Delta_M} \qquad (100a)$$

while

$$\alpha_i^- \simeq \frac{1}{2} \left(\frac{\delta_M}{\Delta_M} \right) . \qquad (100b)$$

It follows from equations (100a and b) that α_i^+ is an entrance angle close to 90° while α_i^- is an entrance angle close to 0°. Physically these two angles are seen to be a consequence of the fact that a small δ_M may be obtained by either letting τ_M get very small or by letting T get very large. The former case implies that p_c would be very small, thus requiring the z-component of the initial momentum to be very small as well, while in the latter case a very small initial radial momentum requires a long transit time t. Finally it should be noted that both α_i^+ and α_i^- approach $\pi/4$ as δ_M approaches its upper limit Δ_M. Since the transmission efficiency of impulsive field mass analyzers is directly proportional to the pulse repetition frequency ν_c (see equation 119), an injection angle $\alpha_i = \pi/4$, and a duty cycle at mass M of Δ_M optimize the performance of the mass analyzer. Further with $\alpha_i = \pi/4$, the term ϵ_2 appearing in equation (91) becomes $2\Delta\alpha_i$ which turns out to be the magnitude of the angular spread of the incident ion beam. $\Delta\alpha_i$, however, is readily controlled by using collimating apertures at the entrance slits S_o. The previous calculations are all based on the assumption that ions in the impulsive region are only deflected once. It is possible, however, for ions having mass $m > M$ to be deflected through an angle $\alpha_f = \pi/2$ after having been deflected n times within the impulsive field region. The collected ions thus give rise to an nth order mass spectrum. The mass peaks, however, appear in erroneous positions on the mass scale of the first order mass spectrum. If the order n can be established, however, nth order spectra may be used to extend the useful range of the mass analyzer.

From an experimental viewpoint, this mass analyzer has an important advantage over the other impulsive mass analyzers, as it requires no separate energy analyzer. Consequently the mechanical and electronic hardware is simplified. The only parts that need careful alignment are the slits S_o and S_e. These slits, of course, limit the sensitivity of the analyzer. The sensitivity, however, may be enhanced if, instead of slits S_e, optically aligned grids spaced at regular intervals b are inserted in front of the collector. If n is the number of such grids having a mesh size of s holes per cm, then it follows from a purely geometrical consideration that the maximum deviation from the final trajectory angle α_f will be 1/sb as long as the collector subtends a solid angle smaller than Ω_c where Ω_c is given by

$$\Omega_c \sim \frac{\pi}{(bs)^2} . \qquad (101)$$

The numerical values of s and b must be chosen on the basis of a compromise between maximum transparency and allowable angular deviation.

The retarding field impulsive mass spectrometers that have been discussed and evaluated are, of course, only a few examples of a large family of such spectrometers. The direction of further inquiry into other possible configurations has, however, been indicated.

4. Accelerating-Field Constant-Momentum Mass Spectrometers

The mass spectrometers listed in Fig. (11) all belong to the general class of accelerating-field constant momentum mass analyzers (CMMA). The instruments may be divided into two groups - gated and ungated mass analyzers. The gated instruments have an ion buncher in front of the impulsive field region the purpose of which is to inject

an ion bunch into the impulsive field at the instant the pulse voltage is turned on. This insures that no ions leave the impulsive field while the pulse voltage is on. The ion energy analysis of the ions emerging from the impulsive field region may be carried out with a simple retarding voltage placed in front of the ion collector. Two types of gated mass analyzers have been evaluated in previous publications[2,3]. The ungated mass analyzers require a more sophisticated ion energy analysis, since ions located beyond a critical distance from the first grid (grid No. 1 in Fig. 10) leave the impulsive field before the pulse voltage is turned off. These ions have a range of energies adding an undesirable background to the energy spectrum. This background may be minimized by using an energy analyzer which may be tuned to a particular energy. Consequently the EEA is the appropriate energy analyzer for the ungated mass analyzer.

There are two ways of obtaining a mass spectrum from a mass analyzer consisting of an impulsive accelerating field region and an EEA: one may fix the time duration τ of the pulse $V_c(t)$ and then sweep the voltage applied across the EEA, or one may keep a constant voltage across the EEA and vary the time duration τ of $V_c(t)$. The former mode of operation has the disadvantage that the mass sensitivity of the mass spectrometer varies inversely with the mass of the ions, since the usable fraction of ions located within the pulse region becomes small for the light ions. Its single advantage lies in the fact that only a free running pulse generator and a ramp function generator are required. The latter mode of operation has the advantage that the mass sensitivity is not as strongly dependent upon the ion

mass over the chosen mass range, since the distance traversed by the ions inside the impulsive field region while the pulse voltage $V_c(t)$ is on is independent of the mass of the ions. A more thorough discussion of this point follows. Experimentally this mode of operation may be realized by using a pulse generator with a pulse voltage output, the time duration τ of which may be controlled by an applied voltage $V_R(t)$ such as a ramp function (see appendix). The ramp function is simultaneously applied to the horizontal axis of either an X-Y recorder or an oscilloscope, while the y-axis is connected to an electrometer. Fig. (15) shows the essential features of this mode of operation. In order to calibrate the mass analyzer it is necessary to obtain τ as a function of m and E_i. $\tau(m,E_i)$ may be derived from equation (3), with the minus dropped since the ions are accelerated, into which equation (86) is inserted to obtain

$$\frac{b}{m}\tau^2 + 2\sqrt{E_i \frac{b}{m}}\,\tau - (E_f - E_i) = 0 \qquad (102)$$

Solving equation (102) for the roots $\tau(m,E_i)$ one finds that

$$\tau(m,E_i) = \sqrt{m}\left(\frac{\sqrt{E_f}-\sqrt{E_i}}{\sqrt{b}}\right). \qquad (103)$$

Note that the parameters E_f and E_i are fixed - the former by the choice of voltages across the EEA, and the latter being determined by the ion source conditions.

Consider equation (102). A Taylor-expansion of $E_f(\tau)$ about τ yields the following after simplifying with equation (86)

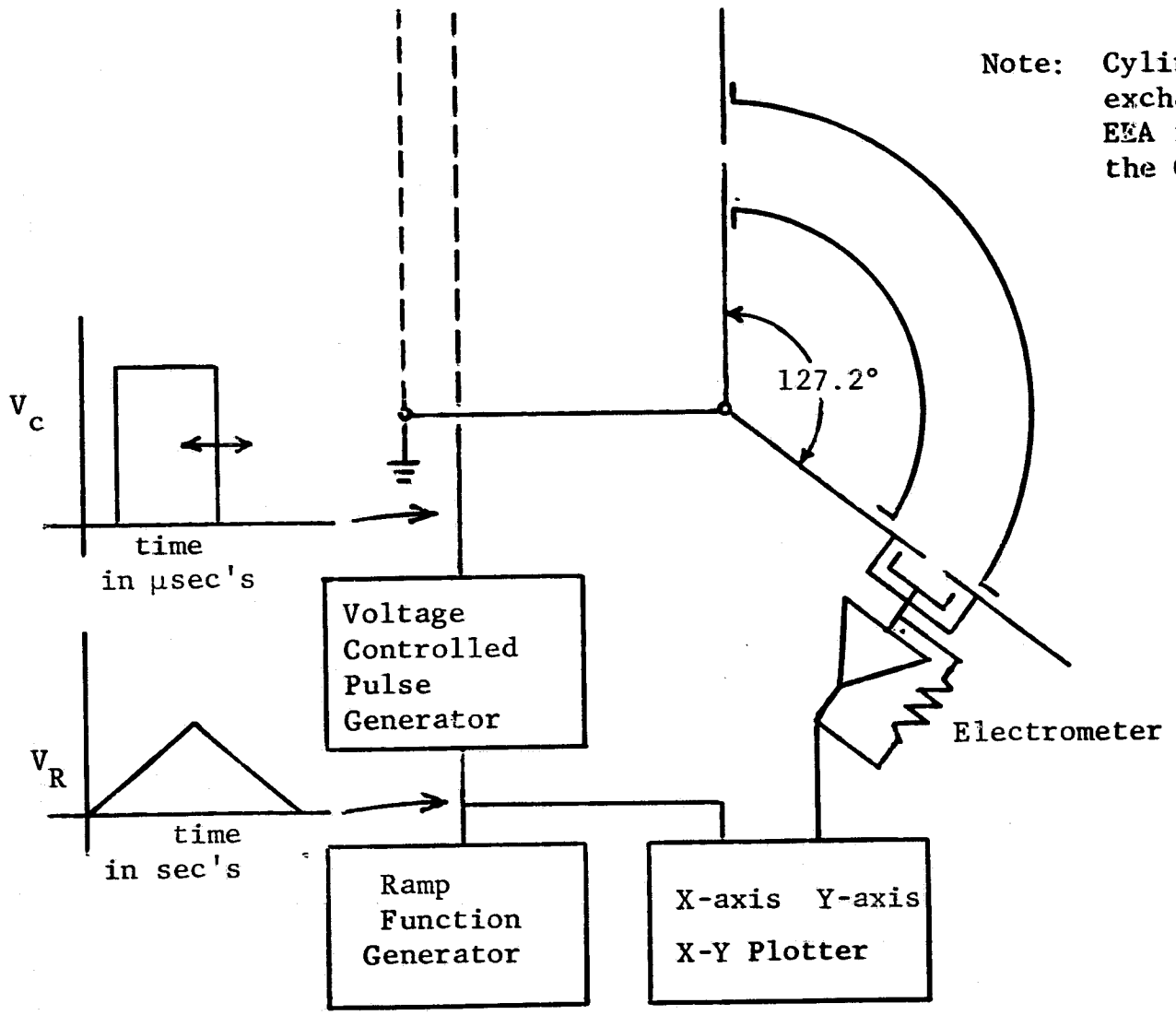

Note: Cylindrical EEA has been exchanged with spherical EEA in later versions of the CMMA.

Fig. 15 Block Diagram of CMMA

$$E_f(\tau + \Delta\tau) = E_f(\tau) + 2E_c \left(1 \mp \sqrt{\frac{E_i}{E_c}}\right) \frac{\Delta\tau}{\tau} + \ldots \quad . \qquad (104)$$

From equations (103) and (86) it follows that

$$E_c = \left(\sqrt{E_f} - \sqrt{E_i}\right)^2 . \qquad (105)$$

Thus inserting equation (105) into the expression for $E_f(\tau + \Delta\tau) - E_f(\tau)$ one obtains to the first order in $\Delta\tau$

$$\Delta E_f = E_f\left(1 - \sqrt{G}\right) \frac{2\Delta\tau}{\tau} \qquad (106)$$

where $G = E_i/E_f$.

Consider now the expression for the resolving power R(m) given by equation (76). Combining equations (76) and (105) yields

$$R(m) = \frac{E_f(1 - \sqrt{G})}{\epsilon} , \qquad (107)$$

hence letting $\epsilon = \left[\Delta E_f\right]_m$, the width of a mass peak at mass m,

$$R(m) = \frac{1}{2}\left(\frac{\tau}{\Delta\tau_m}\right). \qquad (108)$$

Similarly insertion of equation (105) into the expression for $R(m,\Delta E_i)$ given by equation (77) yields

$$R(m,\Delta E_i) = \frac{R(m)}{1 + R(m)\left[\dfrac{\Delta E_i}{\sqrt{E_i E_f}(1-\sqrt{G})}\right]} . \qquad (109)$$

Note here that $R(m,\Delta E_i)$ is determined entirely by the instrument, e.g. E_f and E_i are determined by EEA and source condition respectively, while ϵ is determined by the energy resolution of the EEA.

The experimental resolving power $R_{exp}(m)$ may be obtained from the equation

$$R_{exp}(m) = \frac{1}{2}\left[\frac{\tau}{\Delta\tau}\right]_{0.5} \qquad (110)$$

where $\Delta\tau$ is measured at half-height of the mass peak $\tau(m)$.

Two accelerating field CMMA's were constructed. The first instrument combined a 2.5 cm long impulsive field region with the cylindrical EEA described in section II,3. The second combines an impulsive field region of the same length but having an arc-shaped cross section with the spherical EEA also described in section II,3. The ions were collected at the exit slit of the EEA by a Faraday cup[17] connected to an electrometer. The spectra were recorded by a Moseley model 2-D X-Y recorder. The time duration τ of the pulse voltage $V_c(t)$ varied from 0.6 μsec to 2.6 μsec and E_f was set between 50 and 100 eV while E_i was 20 eV. These parameters insured that the mass range of the mass analyzer included the alkali metals from Na to Cs. Li was excluded, since the pulse generator went unstable for τ less than 0.6 μ sec. In Fig. (16) $R_{exp}(m)$ is compared to $R(m,\Delta E_i)$. Curves marked A,A' are $R(m,\Delta E_i)$ and $R_{exp}(m)$ respectively for the CMMA using the cylindrical EEA, while the curves marked B and B' are those for the CMMA with the spherical EEA. The spectrum of the alkali metals obtained with the CMMA using the cylindrical EEA is shown in Fig. (17).

Having determined the resolving power of the accelerating field CMMA, there remains the problem of arriving at an estimate of the transmission efficiency of the CMMA. Let the transmission efficiency η be defined as the ratio of the collector current $I_c(m)$ of ions having mass m and charge e to the ion current $I_o(m)$ of the same ions incident upon the CMMA, thus

	A,A'	B,B'
E_f	70 eV	90 eV
E_i	20 eV	20 eV
ΔE_i	~ 1 eV	2 eV
ϵ	~0.5 eV	~1 eV

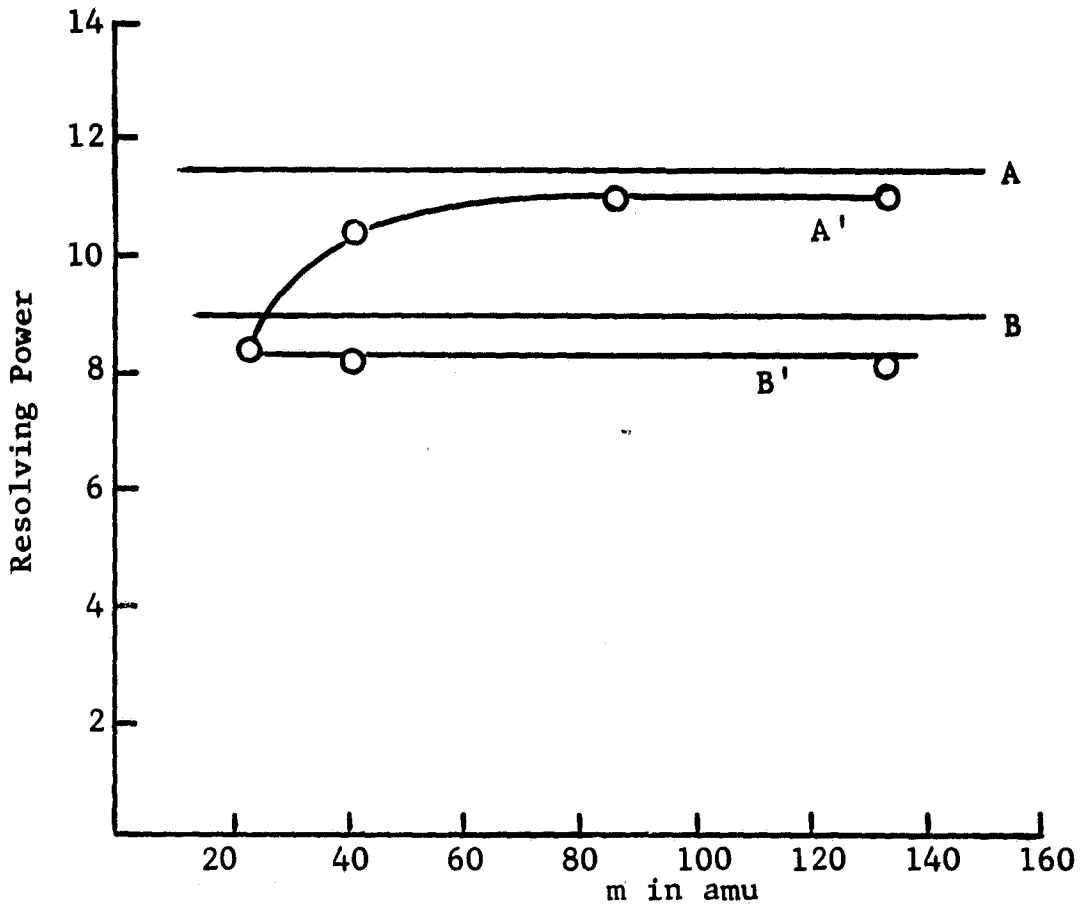

Fig. 16 $R(m,\Delta E_i)$ and $R_{exp}(m)$ for the Accelerating Field CMMA

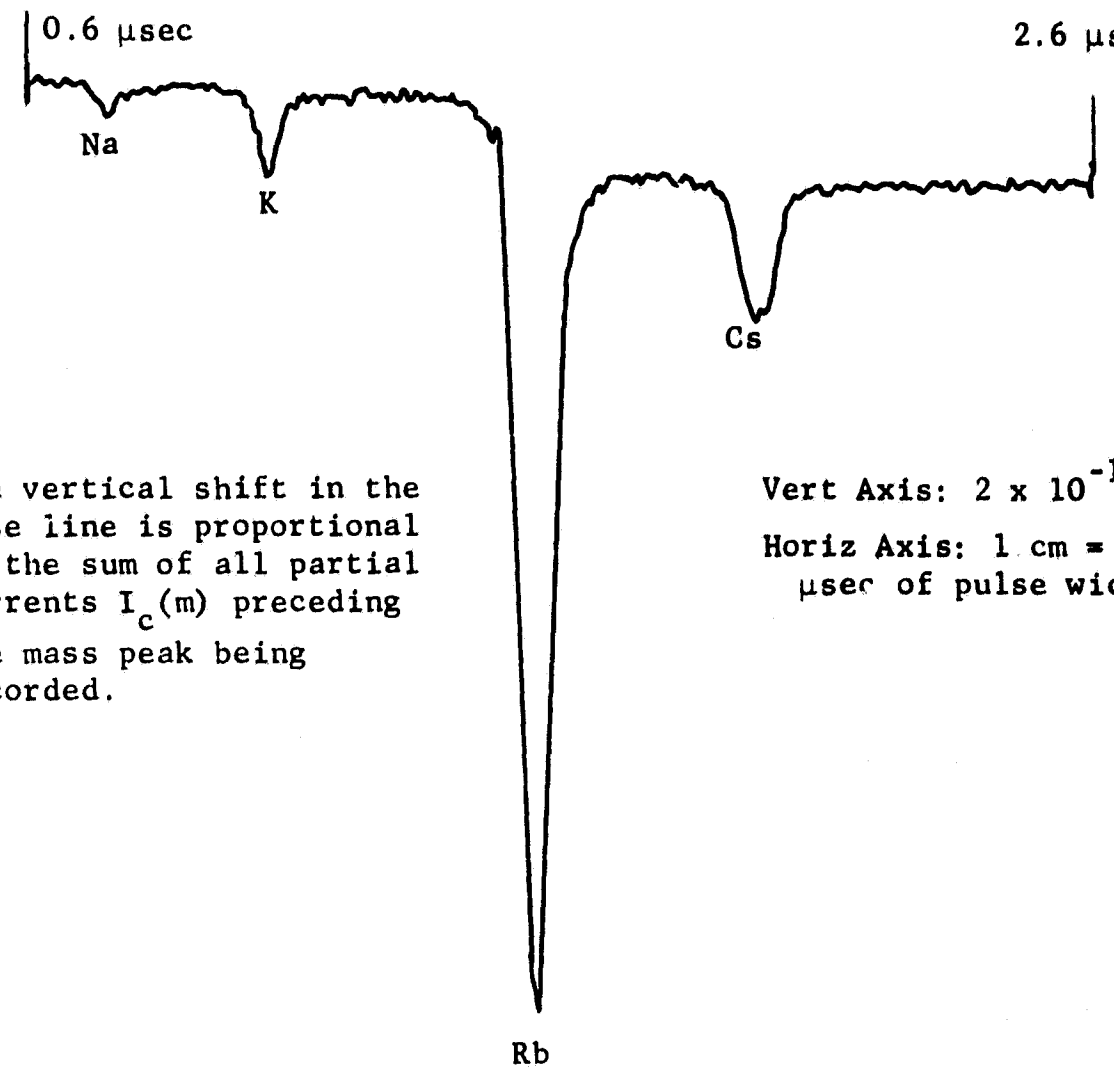

Fig. 17 Mass Spectrum of Alkali Metals Obtained with Accelerating Field CMMA

$$\eta = \frac{I_c(m)}{I_o(m)} \tag{111}$$

In order to simplify the derivation, assume that the ions are mono-energetic having energy E_i, and that the ion current is perfectly collimated - the ion beam incident upon the CMMA having a cross section A. Thus for an ungated accelerating field CMMA, the charge density $\rho(m)$ inside the impulsive field region will be

$$\rho(m) = \frac{I_o(m)}{A}\sqrt{\frac{m}{2\,E_i}} \ . \tag{112}$$

In Fig. (10) let the z-axis be along the axis of symmetry of the mass analyzer, and let z = 0 be the coordinate of grid (1). Consider now an ion at $z = z_c$ the instant that $V_c(t)$ is turned on. Assume that after τ seconds the ion just passes grid (2). Let z_τ be the distance through which the ion accelerated

$$z_\tau = \frac{1}{2}\frac{W_c}{md}\tau^2 + \sqrt{\frac{2E_i}{m}}\,\tau \tag{113}$$

where $W_c = eV_c$ and d is the distance between grids (1) and (2). Hence

$$z_c = d - z_\tau . \tag{114}$$

It follows from equation (114) that all ions located at $z \geq z_c$ leave the impulsive field before the pulse is over. Consequently these ions are lost. The usable fraction of ions are thus contained within the volume for which $z < z_c$, and the number N of ions that receive the required impulsive energy will be

$$N = \frac{\rho(m)}{e} F(d-z_\tau) \tag{115}$$

where F is the cross-sectional area of grids (1) and (2). Let a be

the cross-sectional area of the entrance slit of the energy analyzer (in this case the EEA); then the number n of ions entering the energy analyzer will be

$$n = N \frac{a}{F} \tag{116}$$

Further if 100 percent transmission through the energy analyzer is assumed, the collector current $I_c(m)$ is

$$I_c(m) = e\, u\, \nu_c \tag{117}$$

where ν_c is the pulse repetition frequency. Finally the efficiency η may be derived from equations (111) through (117) to obtain

$$\eta = \frac{a}{A} (d - z_\tau)\, \nu_c \sqrt{\frac{m}{2E_i}} \,. \tag{118}$$

It is apparent that η, given by equation (118), is an upper limit to the transmission efficiency obtainable experimentally, since usually the incident ions are not monoenergetic so that the ions emerging from the impulsive field have an energy distribution $f(E_i,E_c)$ about E_f. If the energy band width of the EEA is(centered about the final ion energy E_f, then only those ions will be collected whose energies lie within the interval $(E_f \pm \epsilon)$. Note that η is a function of the ion mass. This fact was already noted when the two modes of operating the accelerating field CMMA were compared. For the case in which $\tau = \kappa\sqrt{m}$, $(d - z_\tau)$ is independent of m, so that only the $\sqrt{m}$ dependence remains in equation (118).

The calculated transmission efficiency of the accelerating field CMMA, evaluated experimentally, turned out to be 9×10^{-3} for mass 133, other parameters having been listed previously. From the experimental data η was found to be about 4×10^{-3}. The agreement is reasonable;

the factor of two could well be accounted for by the energy spread of the ions emerging from the impulsive field.

The high pressure limit of a mass analyzer is determined by the total flight path and the electric field strength in any part of the instrument. The ion flight path is required to be smaller than the mean free path length of the ions in the mass analyzer, while the maximum field strength sets an upper limit to the pressure above which there exists the danger of field ionization of the background gases. The accelerating field CMMA's evaluated were able to operate at pressures of ca. 7×10^{-4} Torr without suffering a significant loss of either sensitivity or resolving power. Since the operating voltages were reasonably low, there was no danger of breakdown at those pressures. The ability of the CMMA to operate successfully at pressures up to a micron makes it useful as a partial pressure monitor. In the next section other uses of the CMMA will be discussed.

5. Possible Uses for the CMMA

It has been shown in sections III,3 and III,4 that the CMMA may be characterized by: compactness, high sensitivity, simplicity of operation, but low resolving power and a high sensitivity to the initial ion energy spread. Consequently the mass analyzer is useful in any mass analysis program in which a high degree of reliability is required, but the resolving power is not critical. One such program is rocket-borne mass analysis of the lower E and upper D region of the ionosphere. In these regions the pressure varies from 10^{-2} to 10^{-5} Torr while the thermal energy spread of the ions is no greater than

0.1 eV. With this energy spread one may, according to equation (109), anticipate a resolving power of about 20, which is quite adequate for the analysis of the ion species present in these regions. Other programs may include monitoring of partial pressures within vacuum systems, leak detection, and the observation of chemical reactions by the method of "finger print" spectra.

This study has derived and verified experimentally the equations governing the operation of the constant-momentum mass analyzer. Further work on the CMMA is now needed in order to verify the limits of $R(m,\Delta E_i)$ and η as both the physical dimensions and the operating voltages become large. Such an investigation would be helpful in arriving at the optimum operating parameters of the mass analyzer.

IV. CONCLUSION

Ions traversing an impulsive electric field region gain or lose an impulsive momentum p_c given by equation (1). This momentum p_c is dependent upon the initial energy E_i and the initial position r_i of the ion within a cylindrical or spherical impulsive field at the instant the field is turned on. In a linear, planar impulsive field p_c does not depend upon E_i or r_i. A planar accelerating impulsive field broadens any initial ion energy spread ΔE_i of ions in a beam traversing the field, while a planar decelerating field decreases the width ΔE_i. The latter field tends to defocus the ion beam traversing it.

The energy analyzer based on the simple retarding field requires a strongly collimated ion beam incident upon it and a small inter-electrode dimension d (equation 45). The simple retarding field in combination with an energy band-pass filter has found application as an ion energy analyzer in order to measure ion energies E' in the interval $E = eV_r \leq E' \leq E_u$, where both E and E_u are determined by the potentials applied to the retarding field and the band-pass filter, and the parameter Θ as shown in Fig. (4). Ion current losses within the energy analyzer are minimized when $\Theta = 45°$.

Experimental evidence suggests that very sensitive, compact cylindrical and spherical electrostatic energy analyzers can be constructed for energy analysis of ions emerging from an impulsive field. The energy analyzers are shown in Figs. (6) and (7). Operating parameters of the above analyzers are tabulated in Fig. (9).

Constant momentum mass analyzers, CMMA's, using a linear, planar accelerating or decelerating impulsive field and an energy analyzer have been shown to achieve a mass resolving power between 10 and 20 for ion energy spreads of widths between 1 and 2 eV. Decelerating field CMMA's require ion energy analyzers having a high resolution at very low energies. The deflection field CMMA shown in Fig. (14) meets this requirement by only allowing ions having energies located closely about the energy kp_ρ^2/m associated with the axial component p_ρ of the initial ion momentum to reach the collector. CMMA's consisting of an accelerating impulsive field having a pulse duration τ given by $\tau = K\sqrt{m}$ were found to have an experimental resolving power in close agreement with the predicted resolving power given by equation (109). The above mode of operation has the additional advantage that the current efficiency η is only weakly dependent upon the mass of the ions.

The three distinguishing characteristics of the CMMA (its simplicity, high sensitivity, but low resolving power) suggest its use in mass analysis programs outlined in section III,6.

APPENDIX

Swept Pulse Width Pulse Generator for Impulsive Mass Analyzers

Fig. 18 shows the circuit diagram of a pulse generator capable of delivering a 100 V square pulse into a capacitive load of about 100 pf at a pulse repetition frequency of 60 KHz. The time duration τ of the pulse may be controlled by a ramp function voltage $V_r(t)$ internally generated. The internal ramp function generator also drives an X-Y recorder at a rate which is adjustable from a sweep time of 3 seconds to approximately 10 seconds by varying the integrating capacitor C_r on the ramp function generator from 0.5 μf to approximately 1.0 μf. The pulse repetition frequency ν_c is fixed by the astable multivibrator Q_1 and Q_2, the master clock of the pulse generator. The output pulse from the clock is differentiated and clipped to obtain a negative going spike. This spike is inverted and amplified by the transistor Q_3. The positive spike from the collector of Q_3 triggers a monostable multivibrator consisting of Q_4 and Q_5 the output pulse width of which is linearly dependent upon the voltage $V_r(t)$ applied to the base of Q_4. In order to reduce the risetime of the input pulse of the high voltage driver Q_6, the clock pulse is added to the output pulse of the multivibrator at the base of Q_6. The resultant pulse rises more sharply than could be obtained by using the output pulse from the monostable multivibrator alone. This arrangement has the added advantage that the pulse voltage at the base of Q_6 does not vary with τ the pulse duration. The output pulse of the high voltage

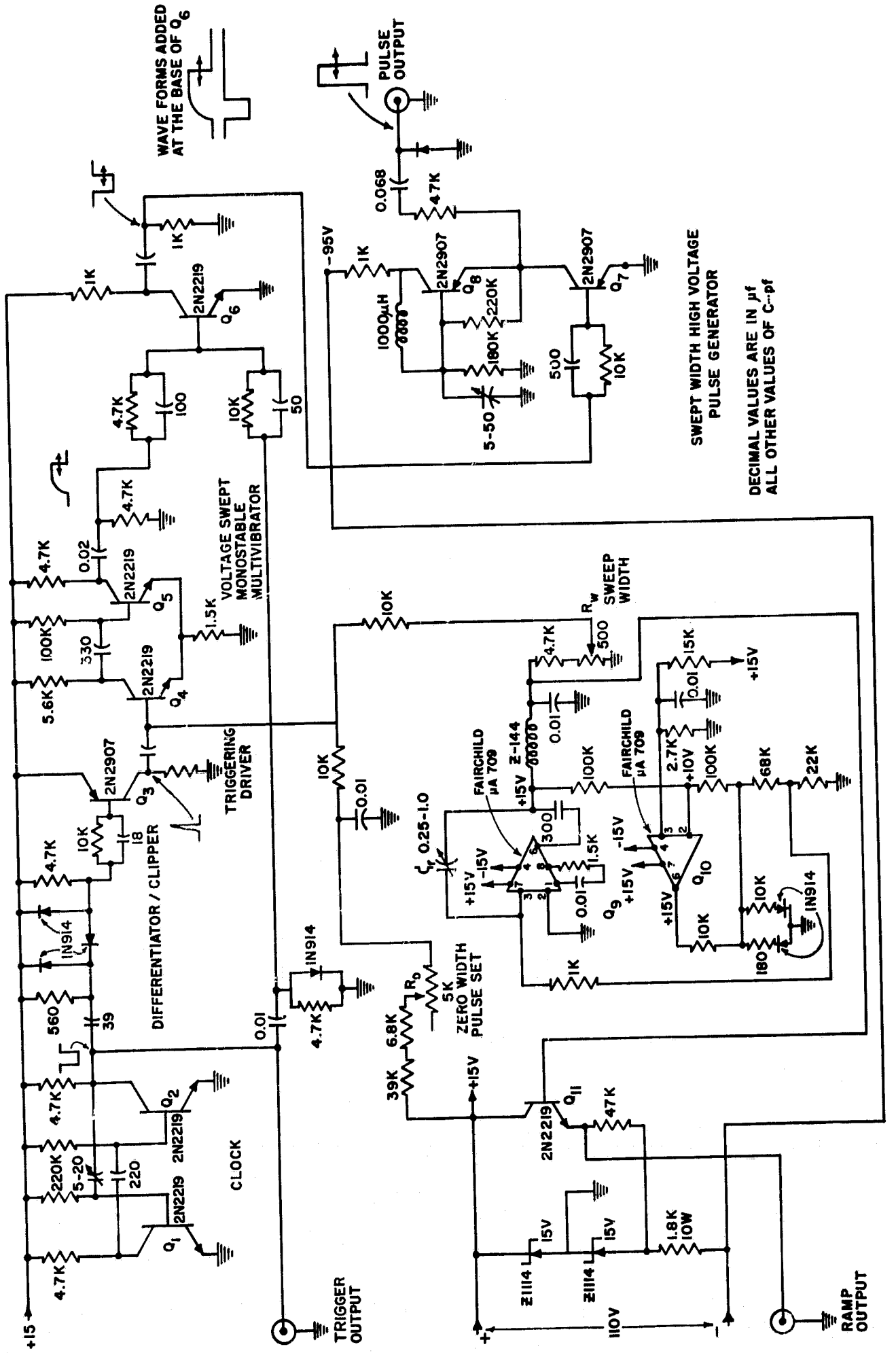
WAVE FORMS ADDED AT THE BASE OF Q_6
PULSE OUTPUT
SWEPT WIDTH HIGH VOLTAGE PULSE GENERATOR
DECIMAL VALUES ARE IN μf
ALL OTHER VALUES OF C--pf
VOLTAGE SWEPT MONOSTABLE MULTIVIBRATOR
TRIGGERING DRIVER
DIFFERENTIATOR / CLIPPER
CLOCK
TRIGGER OUTPUT
ZERO WIDTH PULSE SET
SWEEP WIDTH
FAIRCHILD μA 709
RAMP OUTPUT
2N2219
2N2907
1N914
Z1114 L
110V
+15
-95V
-15V

driver Q_6 is applied to the final pulse amplifier Q_7 and Q_8. These two transistors are connected in series in order to obtain a resultant pulse height approximately twice that of one transistor alone. The positive going output pulse from the final amplifier has an amplitude of 100 V, a risetime of 100 nsec and a decay time of about 300 nsec when the generator is connected to a load having a distributed capacitance of approximately 100 pf.

The integrated circuits Q_9 and Q_{10} together furnish the ramp voltage $V_r(t)$. Q_{10} is used as a Schmitt trigger, while Q_9 functions as an integrator of the output voltage from Q_{10}. This voltage is applied to Q_4 and an emitter follower amplifier Q_{11} which provides the necessary impedance matching for the X-Y recorder. Finally R_w and R_o set the upper and lower limits of $V_r(t)$ which in turn determines the range of τ. Typically R_o and R_w are adjusted to give τ a range from 0.7 μsec to 3 μsec. There is a slight interaction between adjustments.

BIBLIOGRAPHY

1. W. M. Brubaker, Proceedings of the ASTM-E14 Conference, Dallas, Texas, May 1966, p. 528.

2. H. M. Luther, B. R. F. Kendall, Proceedings of the ASTM-E14 Conference, Dallas, Texas, May 1966, pp. 369-372.

3. H. M. Luther, Scientific Report No. 283, Ionosphere Research Laboratory, The Pennsylvania State University, Nov. 1966.

4. B. R. F. Kendall, H. M. Luther, Am. J. Phys. 34, 580, (1966).

5. I. E. Dayton, et al. Boeing Scientific Laboratory's Report No. DI-82-0508. Clearinghouse for Federal Scientific and Technical Information; Report No. A.D. 634-235.

6. V. E. Cosslett, Electron Optics, Oxford, Clarendon Press, 1950.

7. H. Wollnick, Focusing of Charged Particles, A. Septier ed. Vol. II, p. 163 ff. Academic Press, New York, London, (1967).

8. H. Ewald, H. Liebl, Z. Naturforschg. 10a, 872-876, (1955).

9. H. Ewald, H. Liebl, Z. Naturforschg. 12a, 28, (1956).

10. J. A. Hipple, U. S. Patent 2,764,691 Filed August 3, 1953.

11. V. B. Fiks, Soviet Phys. (Doklady) 1, 89, (1956).

12. W. M. Brubaker, U. S. Patent 2,157,985 Filed June 5, 1958.

13. M. M. Wolff, W. E. Stephens, Rev. Sci. Inst. 24, 616-617, (1953).

14. B. R. F. Kendall, Bulletin of the Radio and Electrical Engineering Division, National Research Council of Canada 9, No. 2, 22, (1959).

15. B. R. F. Kendall, Bulletin of the Radio and Electrical Engineering Division, National Research Council of Canada 10, No. 1, 25, (1960).

16. J. Bracher, Zeit. Angew. Phys. 19, 347, (1965).

17. W. R. Miller, N. N. Axelrod, Rev. Sci. Inst. 37, 1996, (1966).